ADVANCES AT AEDC IN TREATING TRANSONIC WIND TUNNEL WALL INTERFERENCE*

by

E. M. Kraft† and A. Ritter‡
Calspan Corporation / AEDC Division
and
M. L. Laster§
Directorate of Technology
Deputy for Operations, AEDC

SUMMARY

The Arnold Engineering Development Center (AEDC) has had a continuous program to develop techniques to determine or minimize the effects of wall interference in wind tunnel tests of three-dimensional aircraft at high transonic speeds. Advances in three major technologies have evolved from this program:

i) pretest predictions of 3-D transonic wall interference are now routinely performed for production wind tunnel tests using advanced numerical techniques and an improved mathematical description of perforated walls,

ii) *in situ* wall interference assessment/correction techniques have been developed for 3-D transonic flow and a preliminary evaluation using numerical simulations has been performed, and,

iii) a 3-D variable-porosity adaptive wall system has successfully eliminated wall interference at near sonic conditions.

The basic development and status of each of these technologies is summarized in this paper.

---

*The research reported herein was performed by the Arnold Engineering Development Center (AEDC), Air Force Systems Command. Work and analysis for this research was done by personnel of the Calspan Corporation / AEDC Division operating contractor for aerospace flight dynamics testing at AEDC. Further reproduction is authorized to satisfy the needs of the U.S Government.

Acknowlegement is given to the major contributors to the research reported herein - Dr. J. C. Erickson, Jr., R.L. Parker, Jr., W.L. Sickles, Dr. J.L. Jacocks, and Dr. J.A. Benek of the Calspan Corporation / AEDC Division. Their individual contributions are noted throughout the paper.

† Assistant Branch Manager, Aeromechanics Branch, Propulsion Wind Tunnel Facility.
‡ Director of Technology
§ Technical Director

1.0 INTRODUCTION

Wind tunnel wall interference has been recognized as a potential source of error in aerodynamic developmental testing almost since the first wind tunnel data were obtained. One of the first wind tunnel-to-flight correlations was done by G. I. Taylor (as recounted in Ref. 1) and the correlation produced reasonable results only after the wind tunnel data were adjusted for blockage effects. Some of the writings of aerodynamic pioneers like Prandtl (Ref. 2) and von Karman (Ref. 3) reflect their awareness and interest in this problem. Prandtl's lifting line theory was an important catalyst for the development during the 1920's and 30's of rather comprehensive wall interference theories for solid wall and open jet wind tunnels. Theodorsen's work (Ref 4) clearly established that wall interference could be minimized by a mixed (partially open and closed) boundary. Of course, the work of Stack and his colleagues (Ref. 5) in the 1940's showed that such a ventilated wall not only reduced wall interference but was necessary to permit tunnel operation through the speed of sound.

Much developmental work was done in the 1950's to refine the ventilated wind tunnel wall. Emphasis at AEDC was on the perforated hole walls and a complete summary of this work is given in Ref. 6. One of the concepts to emerge from these developments was the 60-deg inclined hole wall which is currently used in all the AEDC transonic wind tunnels. A typical wall pattern is illustrated in Fig. 1. The primary theoretical developments in wall interference during the 50's and 60's was an extension of the earlier concepts for solid-wall and open-jet tunnels to tunnels with either the perforated hole or slotted walls. These developments are summarized in Refs 7 and 8. All of this theoretical development was based on subsonic, linear theory.

In the early 1970's, two major technical advances provided a new impetus to wall interference technology. First, rapid advances were made in computational fluid dynamics (CFD) and calculations of nonlinear transonic flow with embedded shock waves became practical. Second, new insights were gained into the understanding and treatment of wall interference through the adaptive wall concept developed independently by Ferri and Baronti (Ref. 9) and Sears (Ref. 10). The adaptive wall concept was

revolutionary in that it clearly established that a complete definition of wall interference is contained in the distribution of two flow variables measured near the tunnel boundary. This insight also spawned passive methods for wall interference assessment/correction (WIAC) techniques that could be applied to any wind tunnel.

AEDC has had an extensive technical effort to develop these advanced wall interference technologies for implementation in transonic wind tunnels. Because AEDC's transonic testing mission is primarily for military aircraft, the objective has been to develop the techniques for three-dimensional configurations at high transonic speeds. In this paper, observations of wall interference effects at these transonic conditions are made. Moreover, the advances that have been made in wall interference prediction methods, WIAC techniques, and the development of the ventilated adaptive wall concept are presented.

2.0 SOME OBSERVATIONS OF TRANSONIC WALL INTERFERENCE

In many wind tunnel tests, wall interference is dismissed as unimportant because it is generally assumed that if the model is small enough (i.e., blockage less than one percent) the wall interference is negligible. Many times, if incremental tests are performed, any wall interference that exists is presumed to be common to the various configurations tested and hence is removed when the increments are determined. In addition, wall interference is generally assumed to be independent of other wind tunnel parameters, for example, the Reynolds number. Hence when the wind tunnel data base is extrapolated to full-scale conditions, wall interference is not included in the extrapolation. From time to time, AEDC has had the opportunity to test systematically various models in the 4-foot (Tunnel 4T) and 16-foot (Tunnel 16T) transonic wind tunnels. These tests have provided valuable insight into the nature of wall interference at transonic speeds. In this section, some observations made from these tests and the lessons learned will be summarized.

MODEL SIZE EFFECTS

In Fig. 2, the experimentally measured lift interference on a series of different models is conveniently presented as the classical upwash interference factor, δ_0, which is in effect a normalized angle-of-attack error induced by the wind tunnel walls. The upwash factor was determined by taking the difference in the lift-curve data in Tunnel 4T from the lift-curve data in Tunnel 16T (assumed to be interference-free) at a fixed value of C_L.

One can see from Fig. 2 that, even for models well below the standard one-percent blockage criteria, there is measurable lift interference for $0.8<M<1.0$. The significance of the lift interference factor in Fig. 2 is best illustrated by examining the potential influence of the wall interference induced error in angle of attack on the performance of an aircraft. The error in angle of attack is

$$\Delta\alpha = 57.3\,(A_w/A_t)\,\delta_0 C_L, \text{ degrees}$$

where A_w is the wing reference area, A_t is the tunnel cross-sectional area, and C_L the lift coefficient. Hence, for given values of C_L and with $\delta_0 = \delta_0(M)$ from Fig. 2, lines of constant $\Delta\alpha$ can be overlaid on a general aircraft performance map (C_L vs M). This is illustrated in Fig. 3 for the F-111 aircraft using data from a model with blockage less than one-percent. Two particular isoclines of $\Delta\alpha$ are presented on Fig. 3. The first value, $\Delta\alpha = 0.03°$, represents the accuracy in angle of attack required to determine aircraft range within one percent. Clearly, the cruise performance of the F-111 in the transonic range could not be determined to that level of accuracy if the wall interference is not accounted for. The cruise performance of a fighter-bomber aircraft like the F-111 generally would not have such a stringent criteria, but the results of Fig. 3 are suggestive of the impact that wall interference could have on cruise performance of more critical transport configurations.

The second isocline in Fig. 3, $\Delta\alpha = 0.2°$, represents the allowable error in angle of attack which still permits good vehicle stability analysis. To determine this value, a systematic study of error propagation through the six degree-of-freedom equations of motion was made at AEDC to establish the resulting effects on the frequency and half amplitudes of various oscillatory modes. The parameter influence on the short period, Dutch roll, and roll convergence modes was investigated for a typical fighter aircraft. Allowable errors were defined as those which produced changes in the aerodynamic coefficient slopes which would result in less than a 5-percent change in frequency for a 10-percent change in half amplitude for the given motion. The most critical of all the parameters examined was the pitching moment coefficient slope for the short period mode, which, because of its effect on the frequency, limits the tolerable flow angle error to $\pm 0.2°$. Referring to Fig. 3, since the bulk of data required for stability analysis would generally be obtained between the limits of cruise and buffet onset, all the stability data in the range of $0.80<M<1.0$ could be significantly affected because the error induced by lift interference is greater than 0.2° in that region. Of course, in the development of the F-111, wall interference was accounted for by tests in numerous tunnels but the message to be derived from Figs. 2 and 3 is, that if wall interference is ignored simply because the model is less than 1% blockage, significant errors in the data at the high transonic Mach numbers are possible.

On the other hand, it is important to note from Figs. 2 and 3 that, for $M<0.8$, the lift interference is practically negligible even though the model sizes range from 0.6 to 2.5-percent blockage. Thus, the passive inclined-hole walls used in the AEDC tunnels do an excellent job of essentially eliminating the lift interference at the lower Mach numbers and moderate lift coefficients.

INCREMENTAL EFFECTS

Frequently, incremental data are obtained for various configurational changes and then added to baseline data to predict flight performance. Many times the baseline data may even be flight data from a prototype configuration. This is generally a good developmental technique and allows the designer to overcome various shortcomings, including wall interference, in the wind tunnel data. The inherent assumption in this procedure is that effects introduced by the wind tunnel are constant and hence included in the absolute measured values for each configuration tested. Therefore, when increments to the forces and moments are obtained, it is presumed that the errors are cancelled. However, if the wind tunnel effects change with the configuration tested, these errors can be introduced into the incremental data.

Wall interference can change with configurational changes and consequently introduce errors in the incremental data. To illustrate this effect, consider data obtained on the A-10 aircraft in Tunnels 4T and 16T with and without stores. If the increments with and without stores in forces and moments were independent of wall interference, the increments measured in Tunnel 16T would be equal to the increments measured in Tunnel 4T. Another way of saying this is that the wall interference (the difference between 16T and 4T) should be the same with and without stores. That this is not the case is shown in Fig. 4 for the A-10 at $M = 0.75$. In Fig.4, $\Delta\alpha = \alpha_{16T} - \alpha_{4T}$ at a given C_L, $\Delta Cm = Cm_{16T} - Cm_{4T}$, and $\Delta C_D = C_{D16T} - C_{D4T}$. Note that the wall interference effect on drag is approximately 40 drag counts higher with the stores on than with the stores off. Hence, the incremental loads attributable to carrying the stores could be 40 drag counts in error because of wall interference. In this particular case the clean A-10 model had 1.55% blockage and the A-10 plus stores had 2.11% blockage in 4T; hence, large amounts of wall interference were expected. When stores are added to clean aircraft models, frequently the combined blockage can significantly exceed one percent. The experience gained at AEDC suggests that as long as a model configurational change does not create a significant change to the pressure signature of the model at the tunnel boundary, then incremental data are valid. Of course, the only way to guarantee incremental data is to measure the pressure distribution at the wall to verify that configurational changes have not altered the level of wall interference.

REYNOLDS NUMBER EFFECTS

An important observation that has been made at AEDC is that changes in unit Reynolds number can be coupled with wall interference effects. As will be discussed in more detail in Section 3, the fundamental behavior of a perforated wall tunnel is strongly dependent on the boundary layer displacement thickness which in turn varies with unit Reynolds number. To illustrate this effect, again consider data taken with the clean A-10 model at different unit Reynolds numbers in Tunnel 16T and Tunnel 4T. The differences attributable to lift interference at $M = 0.75$ are shown in Fig. 5 for unit Reynolds numbers of 2.2- and 3.6-million. In Fig.5, $\Delta\alpha$ and ΔC_m are defined as in Fig.4, while ΔC_{D_i} is the induced drag coefficient associated with $\Delta\alpha$ (i.e., $\Delta C_{D_i} = \Delta\alpha \cdot C_L$). As illustated clearly in Fig. 5, the lift interference effects vary with unit Reynolds number. Consequently if the variation with Reynolds number of data from 4T were used to extrapolate for Reynolds number effects, the extrapolation would also include wall interference effects, not just unit Reynolds number effects on the model boundary layer. Similar coupling between unit Reynolds number and wall interference has been noted in Refs. 11 and 12.

In conclusion, as illustrated by these observations, wall interference can produce significant errors in transonic wind tunnel data. The use of small models or the acquisition of incremental data does not necessarily eliminate wall interference as Mach number approaches unity Also, it is possible to mistake wall interference effects as "true" Reynolds number effects. Consequently, it is important to be able to determine accurately and to isolate wall interference at transonic speeds. In the next three sections, advances made at AEDC in techniques to handle wall interference will be presented.

3.0 WALL INTERFERENCE PREDICTION METHOD

In designing a wind tunnel test program it is usually desirable to be able to estimate the wall interference prior to the test. Hence, it is important to have the capability to predict wall interference effects. Wall interference prediction methods are based on analytical or numerical descriptions of the test article and the tunnel boundary. In the past, these methods relied on a linear theory of singularities to simulate the model and a homogeneous boundary condition to describe a ventilated wind tunnel wall. The major shortcomings of this approach are that the linear theory is unreliable as Mach number approaches unity and the homogeneous wall boundary condition does not describe adequately the behavior of a perforated wall test section.

Advances in computational techniques have made it possible to remove the restriction of linear analytical techniques. Moreover, studies on ventilated wall behavior, (Ref. 13), have indicated that the characteristics of perforated wall geometries in use at AEDC could be conveniently correlated to provide a sufficiently accurate model of the walls for use with the new computational techniques. Consequently, the tools were at hand to provide an improved approach to predicting wall interference.

NUMERICAL METHOD

The numerical approach used at AEDC is to solve the Euler equations. The Euler method was selected over potential flow methods because it is not restricted by Mach number or test article geometry. An additional, important consideration is that the isolation of wall interference effects in the computation requires an identical computational mesh be used for both the tunnel solution and the free-air solution. The necessary mesh topology required to embed the tunnel region in a larger computational free-air domain is constructed more conveniently for the Euler equation solvers.

The Euler equation solver developed at AEDC by Jacocks and Kneile (Ref. 14) solves the three-dimensional, unsteady Euler equations in Cartesian coordinates using a finite volume approach. The basic numerical algorithm is the explicit predictor-corrector method of MacCormack (Ref. 15). The computational mesh is a spherical mesh generated by a variant of the method of Thomas (Ref. 16). Two coupled Poisson equations are solved to yield interior mesh coordinates from specified boundary coordinates. A typical mesh is illustrated in Fig. 6. A necessary requirement for computing wall interference using numerical techniques is that the mesh be identical for the flow in the tunnel and in free-air. To minimize any gridding effect, the computational mesh for the free-air case is simply the tunnel mesh with points added to its exterior to form a much larger tunnel (effectively unconfined flow).

PERFORATED WALL BOUNDARY CONDITION

In addition to the use of CFD, however, the major improvement in wall interference prediction capability made at AEDC is through the improvement of the perforated wall boundary condition. The classical ventilated wall boundary condition presumes a global description of the perforated wall characteristic. However, the measurements made in Ref. 13 of local flow properties of various ventilated walls indicate that a local specification is necessary. The data of Ref. 13 show that the boundary layer displacement thickness on the tunnel wall is one of the most important parameters to consider in quantifying the wall boundary condition. Moreover, because of the pressure gradients imposed at the wall by the test article, there is a large variation of boundary layer displacement thickness within a ventilated wall test section.

The boundary conditions on the tunnel surfaces account for boundary layer growth over the perforated walls. The boundary-layer influence is used to update both the pressure and normal mass flux boundary values. Zero normal gradients are assumed for density and the other two components of mass flow with energy being calculated from the state equation. The pressure boundary condition is expressed as a deviation from the free-stream pressure,

$$p_{bc} = p_\infty - q_\infty \theta \frac{dCp}{d\theta} \qquad (1)$$

where p_∞ and q_∞ are the free-stream static and dynamic pressure, respectively, and θ is the local flow angle defined such that outflow from the test section is positive. $dCp/d\theta$ defines the characteristic behavior of the perforated wall. In classical approaches, $dCp/d\theta$ is assumed constant over the wall, whereas in the current approach $dCp/d\theta$, as will be shown below, is determined from the local behavior of the boundary layer. The corresponding boundary condition for the normal mass flux is

$$\left(\rho v_n\right)_{bc} = \rho v_n - 2\left(\rho v_n + \frac{d}{dx}(\rho u \delta^* - \rho u \lambda)\right) \qquad (2)$$

where v_n is the velocity normal to the surface, u is the velocity in the streamwise-direction, δ^* is the boundary layer displacement thickness and λ is the wall mass flux also defined as positive for outflow from the test section.

In Eqs. (1) and (2) the values of ρu and θ at the tunnel boundary are provided from the most recent time step of the Euler code. To update the pressure and normal mass flux at the boundary, δ^*, λ, and $dCp/d\theta$ must be correlated with ρu and θ. The correlation of δ^* and λ with ρu and θ is determined from the behavior of the boundary layer at the tunnel wall. An approximate integral form of the continuity equation may be written as

$$\frac{1}{\rho u}\frac{d}{dx}(\rho u \delta^*) + \theta - \lambda = 0 \qquad (3)$$

To complete the correlation, in principle, the streamwise momentum equation of the wall boundary layer is needed. However, experience from Refs. 13 and 17 indicates that θ and λ are related as shown in Fig. 7. This relationship is expressed as

$$\theta - \lambda = 0.125\,\theta\,[4 - \theta(55 + 250\theta)] - 0.002 \qquad (4)$$

With ρu and θ provided from the most recent time step, Eq. (3) can be integrated using Eq.(4) to provide δ^*. The upstream condition required for the integration is provided by a correlation of data from three transonic wind tunnels at AEDC. The correlation, shown in Fig. 8, relates the displacement thickness at the test section entrance to Reynolds numbers and tunnel size

$$Re_{\delta^*} = 0.11\,(Re_W)^{4/5} \qquad (5)$$

Thus, the wall boundary condition is a function of Reynolds number in the sense that the magnitude of δ^* at the test section entrance is dependent on Reynolds number; but the distribution within the test section is assumed independent of Reynolds number. The adequacy of this approach to determine δ^* is illustrated in Fig. 9 where results from Eq. (3) are compared with measurements from Ref. 13.

Finally, the description of the perforated wall requires the correlation of $dCp/d\theta$ with the other parameters. The data of Ref. 13 indicate that the local pressure coefficient and flow angle in the vicinity of a perforated wall are a function of wall porosity (τ), wall thickness (t), hole diameter (d), and boundary layer displacement thickness. These data have been correlated by Dr. James L. Jacocks in the form

$$\frac{dCp}{d\theta} = f\left(\left(\frac{\tau t}{d}\right)^2 Re_{\delta^*}\right) \qquad (6)$$

as illustrated in Fig. 10. The correlation required the introduction of an additional length scale to achieve proper dimensionless groups and the unit Reynolds number was selected. Note that the Reynolds number was not an independent variable in the experiments in Ref. 13. Therefore, the correlation relationship may not be universal. However, for the range of wall parameters included, the correlation is descriptive of the behavior of the AEDC perforated walls. Furthermore, it is reinforced in Fig. 10 that the characteristic behavior of the perforated walls also changes with Reynolds number; i.e., as Reynolds number increases the perforated walls behave as if they were more open.

RESULTS FROM THE WALL INTERFERENCE PREDICTION CODE

The AEDC wall interference prediction code has been evaluated with two- and three-dimensional experimental data and is now applied to production wind tunnel tests. A typical result for the wall interference on a fighter aircraft at M = 0.6 in the AEDC Tunnel 4T is shown in Fig. 11. The measured wall interference increments were determined by direct comparison with interference-free data obtained on the same model in Tunnel 16T. At low angle of attack, the wall interference is negligible as compared to the data precision. However, at higher incidence, the wall interference is measurable and the Euler code predicts the general level very well. By way of comparison, the classical subsonic wall interference prediction methods would underpredict the level of wall interference by an order of magnitude.

Included in Fig. 11 are measurements and predictions of wall interference at two values of Reynolds number. Recall that the calculations are inviscid and Reynolds number enters the predictions only through the porous wall boundary condition, not the model boundary layer. Hence as Reynolds number increases, the walls behave as if they were more open and the magnitude of the "open-jet" type wall interference is increased. This reinforces the observations made in Section 2.

As another example of the utility of the prediction method, computations were made for a transport aircraft tested in Tunnel 16T. During the test program, unit Reynolds number was varied from 2- to 4×10^6. The difference in the pressure distribution at the 78% wing span station because of this unit Reynolds number variation is illustrated in Fig. 12. Also shown in Fig. 12 is the difference in the pressure distribution computed by the wall interference prediction code at the two values of unit Reynolds number. Recalling that the Reynolds number enters the wall interference prediction code only through the tunnel boundary condition, Fig. 12 suggests that the apparent Reynolds number effect may be caused primarily by the change in wall interference. The prediction of wall interference is necessary, in many cases, to interpret properly the trends measured in a wind tunnel.

A primary consideration in using the 3-D Euler wall interference code for predictions, as for any 3-D CFD code, is the issue of mesh resolution. Because shock waves are generally captured over three-mesh points, if the mesh is relatively coarse it can be difficult to resolve the influence of wall interference on the shocks on the wing surfaces. In addition, the mesh generally becomes even more coarse near the tunnel boundaries. Hence it may be difficult to model the influence of the shock wave pressure rise on the crossflow characteristic boundary condition. To resolve questions about mesh resolution versus the accuracy of the porous wall boundary condition, Dr. John A. Benek employed a mesh embedding technique he developed (Ref.18) to predict the wall interference on a 3-D model tested in the AEDC 1-ft. tunnel. By mesh embedding, he effectively increased the mesh from the nominal number of 30,00 mesh points normally used to approximately 300,000 mesh points. By comparison with detailed pressure measurements made near the tunnel boundary in Tunnel 1T, Dr. Benek was able to show that the porous wall boundary condition characterizes the flow accurately near the perforated

walls if the mesh is adequately resolved. Of course, computational time increases considerably with mesh refinement. However, experience at AEDC has shown that even for a relatively coarse mesh, one can confidently estimate the magnitude of the transonic wall interference using the Euler code and local wall characteristics if at least a few static pressure measurements are made near the tunnel boundary. The additional benefits of making near wall measurements will be discussed in the next two sections.

4.0 WALL INTERFERENCE ASSESSMENT / CORRECTION METHODS

In contrast to the prediction method, the wall interference assessment/ correction (WIAC) methods and adaptive wall techniques require *in situ* measurements of flow variables near the tunnel boundaries. The WIAC techniques are derivatives of the adaptive wall concept: in WIAC the measure of wall interference contained in the tunnel boundary measurements is applied directly to assess or correct the data; with adaptive wall methods these same measurements can be used to guide adjustments of the tunnel boundary to reduce or eliminate the wall interference. The WIAC and adaptive wall techniques, although complementary, are discussed separately in this paper.

WIAC approaches can be categorized as one-variable or two-variable techniques dependent upon the number of flow variables measured at an interface near the tunnel boundary. Smith (Ref. 19) classifies these techniques as Schwarz- or Cauchy-type, respectively, based on the mathematical statement of the boundary condition. The one-variable methods generally use measured static pressure distributions at the interface. This measured information must be supplemented by a simulation of the test article to determine the wall interference. In contrast, the two-variable methods make use of static pressure and flow angle and, at least for linear subsonic flows, can avoid simulation of the test article. Of course, the trade-off compared to the one-variable method is the added difficulty of making the measurement of flow angle near ventilated walls. A practical technique for making such measurements will be discussed in Section 5.0 relative to adaptive wall requirements.

Application of WIAC techniques to two-dimensional flows is well established, and the current state of the art for 2-D flow is summarized in Ref. 20. However, the challenge is to extend the WIAC concept to 3-D transonic flows. A major difference between 2-D and 3-D WIAC techniques is that the surface pressure distribution on the model is generally available in 2-D whereas in 3-D only integrated forces and moments are generally available. This difference has a significant impact on the WIAC procedures in 3-D flows. The progress made in 3-D WIAC techniques at AEDC is summarized in this section

ONE-VARIABLE METHOD

Kemp (Ref. 21) was the first to suggest the use of measured wall pressure distributions with a nonlinear transonic code to compute 2-D wall interference, and Murman (Ref. 22) subsequently extended Kemp's concept. Rizk and Murman (Ref. 23) extended the approach to three-dimensional tunnels and developed a computer code, TUNCOR, for this purpose. TUNCOR has been installed on the CRAY computer at AEDC and has been undergoing further development and evaluation under the auspices of NASA Langley Research Center and AEDC.

The basic TUNCOR code provides corrections to Mach number and angle of attack. Lift, pitching moment, and pressure measurements near the tunnel wall are required. The correction procedure may be divided into two steps. First, the flow about the test model is simulated numerically with an inviscid transonic flow code using the pressure measurements near the tunnel walls as boundary conditions. In this step, the wing and tail angles of attack, $\alpha_{T,w}$ and $\alpha_{T,t}$, are determined such that the calculated lift and pitching moment of the simulated model are equal to the measured lift and pitching moment. The angles of attack will generally be different from the experimental values $\alpha_{e,w}$ and $\alpha_{e,t}$ because of viscous effects present in the experiment as well as geometrical differences between the test model and simulated model. In the second step, the flow about the model in free air is simulated numerically. Angle-of-attack corrections and a free-stream Mach number correction are determined such that the calculated model lift and pitching moment match the experimental values, and the calculated Mach number difference on the model surface in the tunnel and free-air is minimized. A summary of the correction procedure is given in Fig. 13.

Preliminary evaluation of the TUNCOR code at AEDC suggested several refinements. One of the major refinements was a conversion of the code to cylindrical coordinates to accommodate the pressure measurements that are made on a cylindrical surface in the AEDC 1T Tunnel. This modification is summarized in Ref. 24. Additional modifications being implemented are: (1) defining a global angle-of-attack correction instead of independent corrections to wing and tail angles of attack, (2) including the body lift to evaluate corrections to angle of attack, and (3) interpreting the wall interference in terms of a correction to the local pressure distribution instead of a correction to angle of attack and Mach number. Detailed numerical simulations have been performed to evaluate the TUNCOR code, and these results wil be discussed below in relation to the two-variable methods.

TWO-VARIABLE METHOD

The accuracy of the single measured variable method is dependent on the accuracy of the model representation. In contrast, by using two measured variables at the interface, it is possible to eliminate the need for representation of the model, at least for subsonic, linear flows. An effective model shape can be determined from the second measured variable. In addition to the pressure distribution, the second variable typically measured is the flow angle. Hence, the two-variable method (TVM) is closely related to the adaptive wall techniques to be discussed in Section 5. The measurement system used to measure pressure and flow angle for WIAC applications at AEDC is the same system described in Section 5 for the adaptive wall.

For subsonic flow, where linear Prandtl-Glauert theory can be used, the wall interference can be determined directly from the two-measured variables without an explicit determination of the effective model shape. This has been clearly shown by Lo (Ref. 25) and Kraft and Dahm (Ref. 26) for two-dimensional subsonic flow. The use of linear theory has also been extended to 3-D subsonic flows at AEDC.

For nonlinear, transonic flows, however, it is necessary to define an effective model shape from the two measured variables. In principle, one can define an arbitrary reference surface surrounding the model and using, say, the measured pressure at the interface, iteratively determine the normal velocity distribution on that reference surface that is compatible with the measured flow angle at the interface. This normal velocity distribution on the reference surface (the equivalent model shape) can then be used in an infinite domain calculation. Comparison of the equivalent body in the tunnel and in free-air then defines the wall interference.

An approach to the transonic two-variable method has been developed by Dr. J. C. Erickson, Jr. Instead of an arbitrary reference surface, Dr. Erickson starts with the test model geometric shape, then adjusts this shape using the measured interface pressure distribution to match the interface flow angle distribution. Straightforward mode shapes, such as a constant, a linear distribution, or square root distribution are added to the geometric shape until the flow angle is matched at the interface. The selection of these mode shapes is guided by simple boundary layer approximations. This approach is equivalent to the two-variable technique described above but with the reference surface collapsed to the model surface. The use of the model surface as the basis for determining the effective body shape is, at the present stage of development, a more robust way to determine the effective body.

Although the approach by Erickson requires the test model shape, the important difference between this TVM approach and the one-variable approach is that the effective shape determined includes an approximation to the viscous effects inferred from the second measured variable. The one-variable technique, such as TUNCOR, uses only the inviscid geometric shape. Of course, if the search for the equivalent shape is bypassed in the two-variable method then the code is equivalent to the TUNCOR code.

EVALUATION OF WIAC TECHNIQUES

To evaluate the 3-D transonic WIAC techniques systematically, a series of numerical simulations has been performed. The flow over a generic wing-body-tail model, illustrated in Fig. 14, was numerically simulated with a transonic small disturbance code in a transonic wind tunnel with an open jet boundary condition, $u = \partial\phi/\partial x = 0$, at the tunnel boundary. This particular model was used in fundamental WIAC and adaptive wall experiments in Tunnel 1T and has a solid blockage ratio of 2.5 percent in Tunnel 1T.

In the numerical simulations of the flow in the wind tunnel, viscous effects on the model wing were included using a simple integral boundary layer theory. Since the test simulations and the WIAC techniques both rely on the same inviscid transonic small disturbance equation solution procedure, the effective body shape determination would be trivial unless the viscous effects are included. Inclusion of the viscous effects on the model also allows a better evaluation of the relative merits of various ways to interpret wall interference corrections.

Traditionally, wall interference effects are interpreted as corrections to the wind tunnel speed (or Mach number) and model angle of attack. The inherent assumption in this approach is that gradients induced by wall interference are negligible. As shown by Ashill & Weeks (Ref. 27) this quite frequently is not the case. An advantage to this approach, however, is that the pressure distribution and boundary layer on the model in the wind tunnel are approximately the correct distributions at the corrected tunnel conditions. Of course, this implies that a corresponding free-air condition exists for the flow established in the wind tunnel. At high transonic speeds this is not necessarily the case.

The alternative to correcting the tunnel speed and model incidence is to correct directly the pressure distribution. Integration of the corrected pressure distribution leads directly to corrected forces and moments at the Mach number and angle of attack defined in the wind tunnel. The advantage with this approach is that strong gradients imposed by the walls are also included. The disadvantage of this approach is the interpretation of the influence of the corrected pressure distribution on the boundary layer. For subcritical, attached flows the influence of the corrected pressure on the boundary layer is probably inconsequential. On the other hand, if strong shocks and/or separation are present, the corrected pressure distribution may infer a different boundary layer on the model. To date, wall interference correction procedures have not attempted to correct simultaneously for an alteration of the boundary layer

between the wind tunnel and flight. At high transonic speeds, the implication is, however, that it may be necessary also to include some sort of boundary layer correction. In either event, a thorough evaluation of WIAC techniques at high transonic speeds also requires a controlled comparison of corrected speed and flow angle versus corrected pressure distribution.

A preliminary assessment of the various WIAC techniques and correction schemes is presented in Fig. 15. For this case, the entire wing-body-tail model was simulated at $M = 0.85$ in an open jet tunnel for numerical convenience. For corrections to the lift coefficient, presented in Fig. 15a, a correction to either tunnel conditions or pressure distribution produces excellent results. However, at $\alpha = 2°$ there is already a suggestion that the two-variable method may give a more accurate correction than the single variable method. Although the results from the TUNCOR code are not displayed in Fig. 15, they are equivalent to the solutions from Erickson's method for the flow condition corrections or the one-variable corrections to pressure shown in Fig. 15. For the numerical simulations performed, it appears that correcting the tunnel conditions provides a better correction for pitching moment as illustrated in Fig. 15b. At this Mach number the flow on the model is mildly supercritical. The implication is that with shock waves present, a more refined interpretation of wall interference on the local pressure distribution, including corrected shock locations, will be necessary for proper correction of the pitching moment. The current 3-D WIAC techniques alter the shock location, but not necessarily in a correct fashion.

A more detailed evaluation of WIAC techniques was performed using a simulation of the wing alone at zero angle of attack. The spanwise distribution of the chordwise rms error in the pressure coefficient as compared to the free-air simulation was evaluated for various WIAC procedures at different Mach numbers. The results are presented in Fig. 16. At $M = 0.70$ and 0.80 it is seen that the residual error in the spanwise pressure distribution is essentially zero if the TVM is used to correct the pressure distribution. This TVM method produces the smallest residual error over the conditions simulated. At $M = 0.86$ the shock waves are stronger and there is a corresponding increase in the residual error of all techniques. This increase in residual error is a direct result of the interpretation of wall interference when there is significant displacement of the shock between the tunnel and free-air conditions wherein the shock/boundary layer interaction changes significantly.

The overall rms residual error in the pressure distribution on the wing versus Mach number is shown in Fig. 17. Correspondingly the overall rms residual error at various angles of attack is shown in Fig. 18 for $M = 0.80$ and 0.86. Clearly, for all conditions simulated, the correction of the pressure distribution with the two-variable method yields the least residual rms error in pressure distribution. There is also an indication that all the WIAC techniques lose accuracy rapidly at the higher transonic Mach numbers suggesting that either the WIAC techniques will be limited in their range of applicability or a more refined interpretation of corrections, which includes the differences in shock location between tunnel and free-air conditions, will be needed.

These preliminary numerical evaluations of WIAC techniques suggest that the two-variable method is preferrable. However, a systematic experimental evaluation of these techniques must be made to confirm the relative merits of the techniques. AEDC is in the process of performing this experimental evaluation using the model shown in Fig. 14. These results will be reported in the future.

5.0 THREE-DIMENSIONAL TRANSONIC ADAPTIVE WALL WIND TUNNEL

It is envisioned that WIAC techniques will be used widely in future transonic wind tunnel testing. However, it is also expected that for some combinations of model and test conditions, tunnel data will be uncorrectable to the free-air case. Consequently, it will be necessary to reduce or eliminate wall interference by adaptation of the tunnel boundaries. The basic concept underlying adaptive wall technology and the accompanying wind tunnel verification for two-dimensional, subsonic flows was presented at the 10th ICAS Congress in 1976 (Ref. 28). Since then considerable progress has been made in the United States and Europe. Today this concept is firmly established and has been well demonstrated for two-dimensional transonic flows.

AEDC began initial research on adaptive wall tunnels in 1975 with two-dimensional experiments. These experiments are summarized in Refs. 29 and 30. However, wind tunnel testing of three-dimensional configurations is the primary test mode at AEDC. Consequently, the technology has been directed toward development of a three-dimensional adaptive wall test section. Moreover, since the primary concern about wall interference is in the high transonic flow regime, the adaptive wall development at AEDC is based on use of perforated wind tunnel walls in view of their excellent shock cancellation characteristics.

Preliminary 3-D adaptive wall experiments were performed in the AEDC Tunnel 4T in 1978 using the four independently variable but uniform porosity walls and plenum pressure to provide, in essence, a five degree-of-freedom adaptive wall tunnel. These early experiments, summarized in Ref. 31, were quite successful but strongly suggested that spatial distribution of porosity control would be necessary to eliminate simultaneously wall interference on the wing and tail. Based on the success of these preliminary experiments, a commitment was made in 1980 to

develop a fully automated 3-D, transonic adaptive wall test section for the AEDC Aerodynamic Wind Tunnel (1T). The essential features of a 3-D adaptive wall test section that had to be developed were the adaptive walls, the interface measurement system, the computational procedure for the external fictitious region, and the control logic for adapting the walls. These features are briefly described in this section. More detailed descriptions of the systems are available in Refs. 32 and 33.

ADAPTIVE WALLS

Since the primary mission of transonic testing at AEDC is directed toward military aircraft that operate near sonic velocity, it was imperative to consider ventilated walls to attenuate pressure waves that reach the tunnel boundaries. A systematic evaluation was performed of various ventilated wall concepts including a slotted wall configuration with variable-angle baffles in the slots, a 5-percent, 60-deg inclined-hole porous wall with segmented plenum chambers, and a variable-porosity configuration with segmented porosity control. Considering the effectiveness of control in the upper transonic Mach number regime and the relative ease of implementation, a 60-deg inclined hole, segmented, variable-porosity configuration was chosen as the best candidate for the 3-D test section walls. The basic design of the variable porosity segments is identical to the global variable-porosity design of the Tunnel 4T walls in that a backside plate for each segment can be independently translated to vary the porosity from 0- to 10-percent. A photograph of the Tunnel 1T adaptive walls is shown in Fig. 19.

INTERFACE MEASUREMENT SYSTEM

A complication of using ventilated adaptive walls is that the requisite measurement of two flow variables cannot be made conveniently on the tunnel wall as can be done for a streamlined wall adaptive test section. In addition, an added complication of a three-dimensional adaptive wall tunnel is the requirement to make rapid, accurate measurements at a sufficient number of locations to define adequately the distribution of two flow variables over a 3-D surface. Various techniques were explored including laser velocimetry, stationary and translating multiple probe arrangements, and two-velocity-component static pipes. Based on considerations of accuracy, speed, and robustness, the static pipe offered the most promise for current applications in a 3-D transonic adaptive tunnel.

In the AEDC adaptive wall development, the streamwise and normal components of the perturbation velocity (or equivalently, the static pressure and flow angle) were selected as the necessary flow variables. These velocity components are obtained from the two-velocity-component pipes as follows. Diametrically opposed pressure orifices are located on a circular cross-section pipe along the direction of the normal to the interface measurement surface as illustrated in Fig. 20. The static pressure is measured at both orifice locations so that, locally, the average static pressure and the pressure difference across the pipe diameter can be evaluated. In effect, this can be regarded as measuring the local static pressure and its normal gradient. The streamwise derivative of the normal velocity $\partial v_n/\partial x$, midway between the two surfaces can be calculated by assuming the flow to be irrotational. The advantage of this measurement technique is that static pressure can be measured precisely, rapidly, and with good spatial resolution. The detailed analysis of this technique is discussed in Refs. 34 and 35.

For the 1T application, it was impossible to mount a sufficient number of pipes in the relatively confined one-foot square test section. Consequently, the interface measurement system is comprised of two static pipes that are mounted diametrically opposed and are rotated so as to describe a cylindrical interface. The pipes are rotated such that the pressure differential is measured and thus the velocity determined in the radial direction. The interface measurement system is illustrated in Fig. 20. This rotating pipe system is necessary in 1T because of size limitations; in a larger wind tunnel an array of fixed pipes would be preferred.

EXTERNAL REGION COMPUTATIONAL TECHNIQUE

The principal theoretical aspect of the adaptive wall method is the evaluation of the functional relationships that satisfy the conditions for unconfined flow in the region exterior to the interface. This requires the solution of a 3-D field exterior to the interface with the distribution of one of the measured flow variables prescribed there as the boundary condition. Previous experience at AEDC demonstrated that the streamwise disturbance velocity is the most effective indicator of required wall control adjustment. Consequently, v_n is used as the boundary condition in the exterior region to calculate the static pressure at the interface which corresponds to the unconfined flow condition. Thus the exterior computational region is well-posed.

The application for the AEDC 1-foot adaptive wall tunnel is in the transonic regime, hence,it is necessary to use a nonlinear transonic computational technique. Because the interface is sufficiently far removed from the model that the disturbances are attenuated, it is sufficient to use the transonic small disturbance equation (TSDE) in the exterior region. The TSDE is generally formulated in terms of the potential , ϕ, but can be defined equivalently for the streamwise disturbance velocity component or acceleration potential, $u = \partial\phi/\partial x$. Since the differential static pipe data yield $\partial u/\partial r$ directly, formulation of the TSDE in terms of u eliminates the requirement to integrate numerically the pipe measurements to provide the boundary condition for the exterior region. This is a major simplification in the use of the pipe data. A careful derivation of the numerical differencing procedure was performed by W.L. Sickles for both the ϕ and u equations in order to assure total consistency

between the two basic formulations. Numerical solutions to either form of the TSDE were obtained by the Murman finite difference method. Agreement between results from both formulations is excellent. Both formulations were implemented as subprogram options in the control algorithm and either can be selected by a prescribed input parameter. Virtually all of the experiments discussed in this paper, however, used the *u* formulation as it is more direct.

ADAPTIVE WALL CONTROL ALGORITHM

A major aspect of the three-dimensional adaptive wall tunnel system has been the development of an automated technique to implement the overall adaptive wall iterative procedure, both accurately and rapidly, without a tunnel operator in the loop. For the ventilated wall concept, the relationship between an adjustment to an individual porosity segment and the resulting change in static pressure on the interface is not confined to the immediate locality of that control. Hence, the relationship between the adjustment of a wall control variable and the response of the flow variable to be set is not a direct one. Therefore, the control algorithm must be capable of directing the adjustments of the wall segments and the plenum pressure to obtain a best fit of the measured interface pressure distribution compared to the desired distribution that results from the exterior calculation.

The heart of the adaptive wall control algorithm is a constrained gradient projection method optimization code. The code used is based on the optimization code first written by Levinsky, *et al* (Ref. 36) for optimizing wing profiles and subsequently modified at AEDC to accommodate more general wind tunnel testing applications (Ref. 37). In the present application, the optimization code was greatly expanded by Dr. J. C. Erickson, Jr., to control the entire adaptive wall iteration process as outlined schematically in Fig. 21. The code is implemented on the host PPD-11/73 minicomputer located in the Tunnel 1T control room and dedicated to these experiments.

Initial conditions for a test are selected and set in the tunnel so that baseline mode interface measurements can be made. As described above, the resulting differential measurement, $\partial u/\partial r$, is used as the boundary condition for the exterior-flow calculation which returns the desired interface pressure coefficient distribution, C_{Pd}, for the first iterative step. The overall control code then evaluates a merit function, Ψ, that is defined as an appropriately weighted integration of the rms difference between C_{Pd} and the measured pressure coefficient distribution, C_{Pm}. Constraints are also defined, if desired, by requiring the equality of C_{Pd} and C_{Pm} at specific points on the interface. The differences between these values are the constraint error functions, g.

At this stage, if Ψ is less than some specified value and if the constraints are satisfied within a specified tolerance, the case has converged, the test is complete, and the model data are interference-free within that tolerance. If not, the tasks continue to make a complete pass through the procedure in Fig. 21.

The next step, if convergence has not been achieved, is to perform the Incremental Mode to determine gradients of Ψ and the g functions with respect to the plenum pressure and wall-control variables. The gradients are found from additional sets of measurements of C_{Pm} at wall settings obtained by perturbing each control variable, in turn, about its Baseline Mode setting. Next, it is checked again to determine if all the constraints are satisfied to within the tolerance. If any one or more of them is not satisfied, a restoration process ensues to bring them to within tolerance. This is accomplished by minimizing the sum of the squares of the individual g functions. If all of the constraints are satisfied, a minimization of the Lagrangian function, which is the sum of Ψ and the product of the g functions and Lagrange multipliers, follows. If there are no constraints, the Lagrangian function reduces to the merit function, Ψ, and it is minimized.

Both the restoration and minimization processes are termed One-Dimensional Searches because they proceed with a constant step-size increment in a single direction. This search direction is defined in terms of specific relationships among the wall control variables that have been found from appropriate operations on the experimentally-defined gradient information. A One-Dimensional Search is continued for the successive steps until the restoration function or Lagrangian function has passed through a minimum. The resultant optimum state at this minimum value is considered to provide the best fit to C_{Pd} and is selected as the next Baseline. As shown in Fig. 21, the procedure is repeated until C_{Pm} and the newly calculated Baseline C_{Pd} agree.

EXPERIMENTAL RESULTS

Initial experiments in the one-foot adaptive wall tunnel were completed in 1983 and are summarized in Ref. 33. The automated features of the test section performed well during these experiments, but convergence to unconfined-flow was not obtained. Subsequent analysis indicated that the accuracy of the interface measurements was inadequate to permit a satisfactory determination of interference-free conditions. During 1984, the interface measurement system was completely redesigned, and a new system was fabricated and installed. After an extensive calibration of the new system, which showed that the desired accuracy of the interface measurements could be achieved, adaptive wall experiments were resumed in January 1985. These recent experiments, performed by R.L. Parker, Jr., and Dr. J. C. Erickson, Jr., are reported below.

The adaptive wall experiments were performed on the wing-body-tail model that has a solid blockage ratio of 2.5 percent. The model was instrumented with 134 pressure orifices located at the positions indicated in Fig. 14. More details about the model and reference

data are contained in Ref. 33. Similar to previous experience at AEDC, measurable wall interference was not observed on the model for M<0.85, even for the high blockage ratio. Hence, all the adaptive wall experiments were performed at Mach numbers of 0.9 and higher.

Merit Function Optimization

In the optimization procedure that adjusts the wall segment porosity and plenum pressure, the merit function is used to describe the relative fit of the measured interface pressure distribution compared to that desired. A typical static pressure distribution at the interface is shown in Fig. 22. Four discrete regions have been identified on the pressure distribution. Regions I and IV are those areas upstream and downstream, respectively, of the model location. Regions II and III are those areas of flow acceleration about the model wing and tail, respectively.

Experiments have shown that it is relatively important to match the measured pressure to the desired pressure in Region I, or to establish the proper Mach number approaching the model. It is extremely important to match the measured and desired pressure distribution in RegionsII and III in order to obtain unconfined data on the model. Matching of the measured and desired pressure is least important in Region IV.

As described, the merit function is an appropriately weighted rms difference between the measured and desired pressure distributions. The experiments revealed that the optimization procedure was highly dependent on the weighting function of the merit function. The earliest experiments employed a uniformly weighted merit function. This form of the merit function placed too much emphasis on Regions I and IV since these regions contribute heavily to the total area between the measured and desired distributions. The results with this merit function form were consequently dominated by global features such as Mach number and gave inadequate attention to local requirements in the vicinity of the model wing and tail.

A more effective form for the optimization procedure was found by defining two separate uniformly weighted merit functions for the wing and tail that spanned Regions II and III, respectively. Subsequent experiments proceeded by conducting two wall optimizations. One addressed the wing requirements using a merit function defined for Region II and one addressed the tail requirements using a merit function defined for Region III. The most effective results obtained to date have been with this individualized merit function strategy.

Control Strategy

One control strategy with the separate merit functions was to minimize the merit function in the wing region and then minimize the merit function in the tail region. The interface pressure distribution for the baseline point, or 0^{th} iteration, for conditions of 0.9 Mach number and a model angle of attack of 4 deg is shown in Fig. 23. Both the measured pressure distribution and the calculated, desired pressure distribution are shown. The data are for an interface azimuthal location of 65 degrees and are typical of the entire interface. The baseline wall configuration is an arbitrary, uniform 3-percent porosity, and the test section Mach number is established by the conventional empty tunnel calibration values. The pressure distribution, after optimizing the wing region merit function, is shown in Fig. 24. The adjustment was accomplished with Mach number control only. The data for the model are shown in Fig. 25. The adjustment resulted in excellent agreement between the adaptive wall data and the reference data from Tunnel 4T for the wing. The tail data were affected adversely by these adjustments as evidenced both at the interface, Fig. 24, and the model, Fig. 25. An attempt to reduce the tail merit function with wall control was unsuccessful.

An alternate control strategy was to minimize the tail region merit function. The interface information after the optimization based on the tail region merit function is shown in Fig. 26. Again, this adjustment was accomplished with only Mach number changes. The model data are shown in Fig. 27. In this case, the wing data have been affected adversely compared to the reference data. For this control strategy, however, wall adjustments were effective in reducing the wing region merit function. This will be discussed later.

These two examples are given to illustrate several points. The consistency between the interface and model information instills confidence in the adaptive wall systems including the static pipes and exterior flow calculations. It is also impressive that simple adjustments in Mach number to match local desired conditions are effective for minimizing interference in discrete portions of the flow field.

However, the longitudinal gradients about a typical wing/tail configuration require longitudinal variation of the boundary condition. These examples also illustrate the conflicting boundary requirements for the wing and tail and, consequently, show why global forms of the merit function proved to be inadequate in previous experiments. The effective manipulation of the wall and Mach number control is highly dependent on the control strategy employed in the optimization procedure.

The control strategy that began with a test section Mach number adjustment, based on the tail region merit function, yielded further improvement when wall porosity control was implemented based on the wing region merit function. The results of the wall adjustments are shown in Fig. 28 for the 65-degree azimuthal interface location. The wall adjustments were effective in providing good agreement between the measured and desired interface conditions in the

wing region. The minimum C_P, or pressure peak, near station 23 is slightly below, or more positive, than that desired. The measured pressure in the tail region does not match the desired pressure as well as the previous iteration shown in Fig. 26, but the tail region was not considered in this iteration.

Converged Results

The results on the model are shown in Fig. 29. The baseline data, which were for uniform 3-percent porosity with Mach number established by the conventional empty-tunnel calibration, are included as well as the previous iteration also shown in Fig. 27. The wall adjustments compensated for the adverse effects of the Mach number adjustment based on the wing region at the interface. There is good agreement overall with the reference data obtained in Tunnel 4T. The model tail data still show good agreement with the reference data even though the match at the interface was adversely effected by the wall moves. This implies that a match of the measured and desired interface conditions in the tail region is a sufficient, but not necessary, condition for unconfined data on the model tail. Apparently the manner in which the interference is manifested in the model tail region is dependent on axial flow gradients in the test section. Allowable tolerance limits on the disagreement between the measured and desired interface conditions have yet to be addressed. It appears as though the tolerance limits might be dependent on the nature of the disagreement instead of simply some constant value of the rms difference.

The results shown in Figs. 28 and 29 were repeatable for the same initial conditions and optimization strategy. The results were also repeatable for different initial Mach numbers. Experiments were started in the same iterative manner for different wall configurations. Measurements appeared to be converging toward the same results. However, this was not verified since the experiments were halted in view of time constraints and facility availability.

At this juncture in adaptive wall development, effective wall control strategy appears to be the critical problem area. The effectiveness of the optimization strategy is strongly dependent on the form of the merit function and the construction of the incremental and One-Dimensional Search Modes. Improvement of the results and ultimate general success of the adaptive wall technique developed at AEDC thus far depends on further refinement and understanding of the optimization strategy.

6.0 STRATEGY FOR IMPLEMENTING WALL INTERFERENCE TECHNIQUES

In routine production wind tunnel testing, data must be obtained rapidly because the cost of testing is a major consideration. Consequently, the implementation of techniques to treat wall interference must be done in a manner consistent with economic considerations. The pretest prediction method does not effect test productivity. On the other hand, WIAC procedures and adaptive wall methods can have a direct impact on the productivity of the wind tunnel and, therefore, must be applied only when required to meet test objectives.

Computation of transonic wall interference by current 3-D WIAC techniques takes approximately twenty minutes on today's supercomputers. Thus it is prohibitive from a cost and productivity standpoint to apply these WIAC techniques on-line to all data points. An appropriate strategy for implementation of WIAC would be to correct selected data in an off-line mode. On-line calculations would be reserved for the assessment of critical data, i.e., those data for which a decision must be made about their quality before the test can proceed. Of course, it is anticipated that improvements in WIAC development, in addition to experience gained through each application, will lead to major reductions in application time.

The computations for the 3-D adaptive wall method are very efficient and take approximately one second on a Class VI computer. In addition, the acquisition of the interface data can be accomplished in less than one second by means of electronically scanned pressure transducers. However, the control logic and iterative cycle, as currently used in the adaptive wall system, can take several minutes. This would prohibit iterative adjustment of the walls for each data point. The proper strategy for implementing the adaptive wall will probably be a fully adapted tunnel for a few critical design points such as the cruise conditon. The adapted wall settings would then be used while the remaining data is obtained. Of course, the interface data can be obtained continually, and on-line assessment or off-line corrections can be made with the WIAC techniques. These selected adapted wall settings could be obtained at the initiation of a test program or even obtained on a small scale, more economical model. It is also anticipated that as adative wall experience is gained for a variety of configurations, there may be optimum wall configurations for classes of models, e.g., transports, fighters, missiles, etc. Small tunnels could be used to gain a data base, inexpensively, to aid in the strategies for application of WIAC and adaptive walls to larger, production wind tunnels.

7.0 CONCLUSIONS

The three major technologies associated with (i) pretest predictions, (ii) wall interference assessment/ correction, and, (iii) adaptive walls, have been developed for three-dimensional transonic flows. Development of the first two at AEDC is directed toward implementation in a production wind tunnel. Further development of the adaptive wall method is dependent on an evaluation of these two technologies.

It is now possible to make pretest engineering calculations of wall interference in 3-D porous wall, transonic wind tunnels. Key advances which make this possible are new CFD techniques for modeling 3-D transonic flows as well as a description of local porous-wall, boundary conditions based on empirical correlations. These pretest predictions are now made routinely to aid in the design of test programs.

One- and two-variable WIAC techniques for 3-D transonic flows have been developed and evaluated by numerical simulations. The final evaluation of these techniques will be based on controlled experiments in the AEDC one-foot transonic wind tunnel. This evaluation will be used to judge the relative merits of one-variable versus two-variable methods as well as the utility of Mach number and incidence corrections versus force and moment corrections. In addition, the experimental evaluation will define the range of applicability of WIAC techniques in the upper transonic regime and so provide a basis for assessing the need for an adaptive wall system. It is expected that a 3-D WIAC technique will be evaluated at AEDC in transonic wind tunnel 4T.

The AEDC one-foot transonic adaptive-wall wind tunnel has been operated successfully near sonic conditons with a generic 3-D wing-body-tail model. Viability of the concept for eliminating wall interference has been demonstrated. However, further refinements in the control strategy of the perforated wall elements are indicated. Strategy for final implementation of this concept will be integrated with WIAC techniques to provide the most cost effective system for minimizing and correcting wall interference.

In the wind tunnel testing environment at AEDC, consideration must be given to tunnel productivity as well as to improving the quality of data. Therefore, added techniques which assess/correct or eliminate wall interference should be used only when required to meet test objectives.

REFERENCES

1. Taylor, G. I., "The Interaction Between Experiment and Theory in Fluid Mechanics" in Annual Review of Fluid Mechanics, Vol. 6, Annual Reviews, Inc., 1974.
2. Prandtl, L. "Tragflugeltheorie, Part II," Nachrichten der K. Gesellschaft der Wissenschaften zu Göttingen, pp 107-137, 1919.
3. von Karman, Th. and Burgers, J. L. "General Aerodynamic Theory - Perfect Fluids" Division E of Aerodynamic Theory, Springer, 1935.
4. Theodersen, T. "The Theory of Wind-Tunnel Wall Interference," NACA Rept No. 410, 1931.
5. Wright, R. H. and Ward, V. G. "NACA Transonic Wind Tunnel Test Sections," NACA RM-L8J06, 1948.
6. Goethert, B. H. Transonic Wind Tunnel Testing. New York. Pergammon Press, 1961.
7. Garner, H. C. *et al* Subsonic Wind Tunnel Wall Corrections. AGARDograph 109, 1966.
8. Pindzola, M. and Lo, C. F. "Boundary Interference at Subsonic Speeds in Wind Tunnels with Ventilated Walls," AEDC-TR-69-47, May, 1969.
9. Ferri, A. and P. Baronti. "A Method for Transonic Wind-Tunnel Corrections," AIAA Journal, Vol. 11, No.1, January, 1973, pp 63-66
10. Sears, W. R. "Self-Correcting Wind Tunnels," (The Sixteenth Lanchester Memorial Lecture), Aeronautical Journal, Vol. 78, No. 758/759; February/March 1974, pp 80-89.
11. Aulehla, F. and Eberle, A. "Reynolds Number Effects on Transonic Shock Location," AGARD CP-335, Paper No. 4, September 1982.
12. Stanewsky, E., Demurie, F., Ray, E. J. and Johnson, C. B. "High Reynolds Number Tests of the Cast 10-2/DOA Transonic Airfoil at Ambient and Cryogenic Temperature Conditions," AGARD-CP-348, Paper No. 10, September 1983.
13. Jacocks, J. L. "Aerodynamic Characteristics of Perforated Walls for Transonic Wind Tunnels." AEDC-TR-77-61 (AD-A040904), June 1977.
14. Jacocks, J. L., and Kneile, K. R. "Computation of Three-Dimensional Time Dependent Flow Using the Euler Equations." AEDC-TR-80-49 (AD-A102463), July 1981.
15. MacCormack, R. W. "The Effect of Viscosity in Hypervelocity Impact Cratering." AIAA Paper No. 69-35, May 1969.

16. Thomas, P. D. "Numerical Methods for Predicting Flow Characteristics and Performance of Nonaxisymmetric Nozzles - Theory." NASA CR-3147, September, 1979.

17. Erickson, J. C., Jr. and Homicz, G. F. "Numerical Simulation of a Segmented-Plenum, Perforated Adaptive Wall Tunnel," AIAA Journal, Vol. 20, No. 5, May 1982, pp. 612-623.

18. Benek, J. A., Steger, J.L., Dougherty, F.C., and Buning, P.G., "Chimera: A Grid Embedding Technique." AEDC-TR-85-64, April 1986.

19. Smith, J. "Measured Boundary Condition Methods for 2D Flow." AGARD CP-335, Paper No. 9, May 1982.

20. Newman, P. A. and Barnwell, R. W., editors. "Wind Tunnel Wall Interference Assessment/Correction." NASA Conference Publication 2319, January 1983.

21. Kemp, W. B., Jr. "Transonic Assessment of Two-Dimensional Wind Tunnel Wall Interference Using Measured Wall Pressures." NASA CP-2045, 1979.

22. Murman, E. M. "A Correction Method for Transonic Wind Tunnel Wall Interference." AIAA Paper 79-1533, July 1979.

23. Rizk, M. H. and Murman, E. M. "Wind Tunnel Wall Interference Corrections for Aircraft Models in the Transonic Regime." Report No. 244, Research and Technology Division, Flow Industries, Inc., Kent, WA, September 1982.

24. Rizk, M. H. "Improvements in Code TUNCOR for Calculating Wall Interference Corrections in the Transonic Regime." AEDC-TR-86-6, March 1986.

25. Lo, C. F. "Tunnel Interference Assessment by Boundary Measurements." AIAA Journal, Vol. 16, No. 4, April 1978, pp 411-413.

26. Kraft, E. M. and Dahm, W. J. A. "Direct Assessment of Wall Interference in a Two-Dimensional Subsonic Wind Tunnel." AIAA Paper No. 82-0187, January, 1982.

27. Ashill, P. R. and Weeks, D. J. "A Method for Determining Wall Interference Corrections in Solid-Wall Tunnels from Measurements of Static Pressure at the Walls." AGARD-CP-335, May 1982, Paper No. 1.

28. Sears, W. R., Vidal, R.J., Erickson, J.C., Jr.,and Ritter, A. "Interference-Free Wind-Tunnel Flows by Adaptive-Wall Technology." ICAS Paper No. 76-02. Tenth Congress of International Council of Aeronautical Sciences, Ottawa, Canada, 3-8 October 1976. Also Journal of Aircraft, Vol 14, No.11, Nov. 1977, pp. 1042-1050.

29. Kraft, E. M. and Parker, R. L., Jr., "Experiments for the Reduction of Wind Tunnel Wall Interference by Adaptive-Wall Technology." AEDC-TR-79-51 (AD-A076555), October 1979.

30. Parker, R. L., Jr., and Sickles, W. L., "Two-Dimensional Adaptive Wall Experiments." AEDC-TR-80-63 (AD-A095199), February 1981.

31. Parker, R. L., Jr., and Sickles, W. L., "Application of the Adaptive Wall Concept in Three Dimensions." Journal of Aircraft, Vol. 18, No. 3, March 1981, pp 176-183.

32. Parker, R. L., Jr., and Erickson, J C., Jr., "Development of a Three-dimensional Adaptive Wall Test Section with Perforated Walls." AGARD-CP-335, May 1982.

33. Parker, R. L., Jr., and Erickson, J. C., Jr., "Status of Three-Dimensional Adaptive-Wall Test Section Development at AEDC." AIAA Paper No. 84-0624, March 1984.

34. Erickson, J. C., Jr., Wittliff, C. E., and Daughtry, D. C., "Further Investigation of Adaptive-Wall Wind Tunnels." AEDC-TR-80-34 (AD-A091774), October 1980.

35. Nenni, J. P., Erickson, J. C., Jr., and Wittliff, C. E., "Measurements of Small Normal Velocity Components in Subsonic Flows by Use of a Static Pipe," AIAA Journal, Vol. 20, No. 8. August 1982, pp. 1077-1083.

36. Levinsky, E. S., et al. "Semispan Wind Tunnel Test Evalution of a Computer Controlled Variable Geometry Wing (Self-Optimizing Flexible Technology Wing Program)," AEDC-TR-78-51, January 1979.

37. Palko, R. L., and Crawford, M. A., "Experimental Verification of an Aerodynamic Parameter Optimization Program for Wind Tunnel Testing," AEDC-TR-81-23, November 1981.

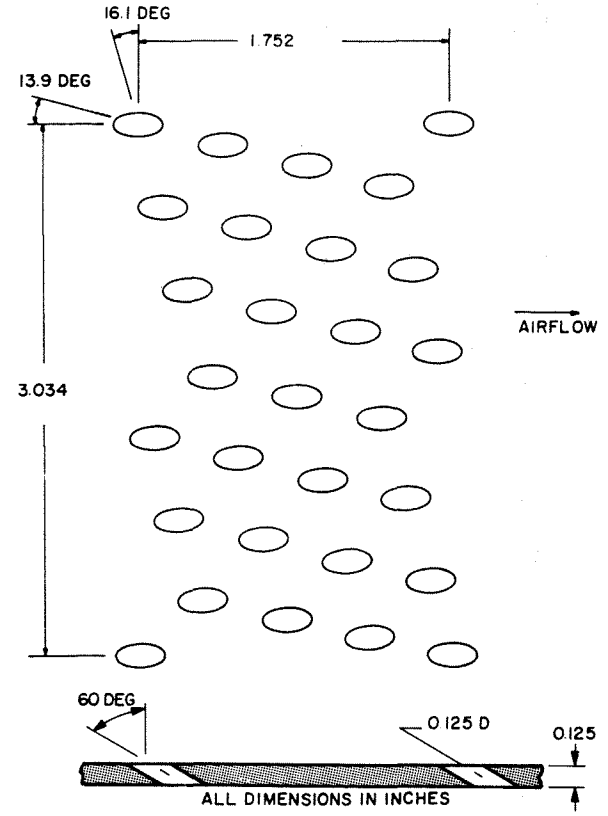

Figure 1. Typical AEDC 60-deg Inclined Hole Wall Pattern.

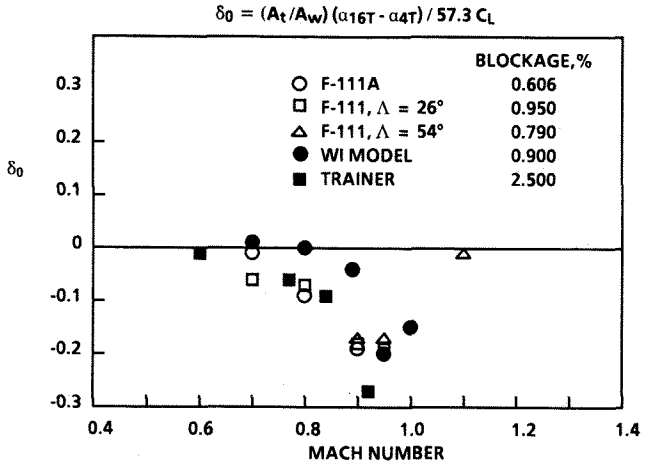

Figure 2. Measured Upwash Interference Factor on Several Sized Models.

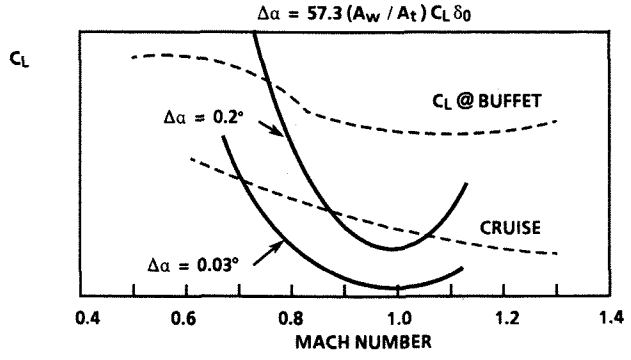

Figure 3. Impact of Upwash Interference on F-111 Performance.

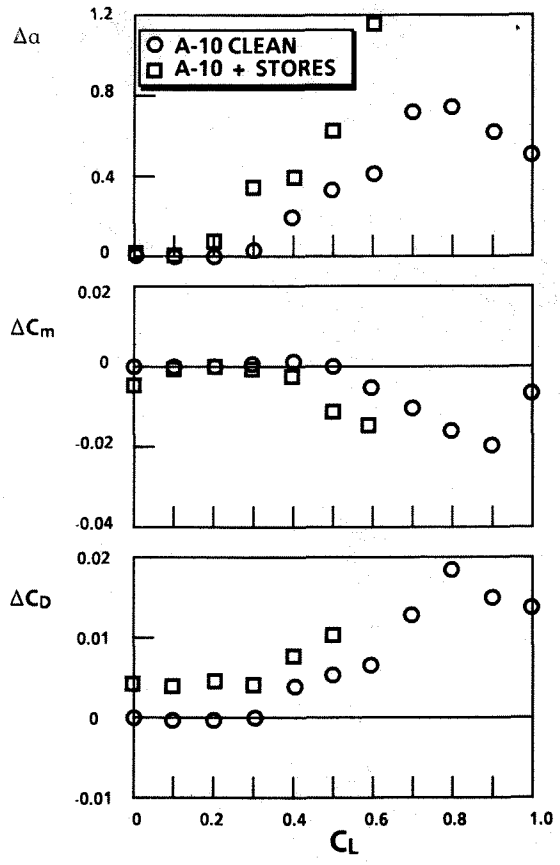

Figure 4. Wall Interference Effects on Incremental Loads for the A-10 Aircraft at M = 0.75.

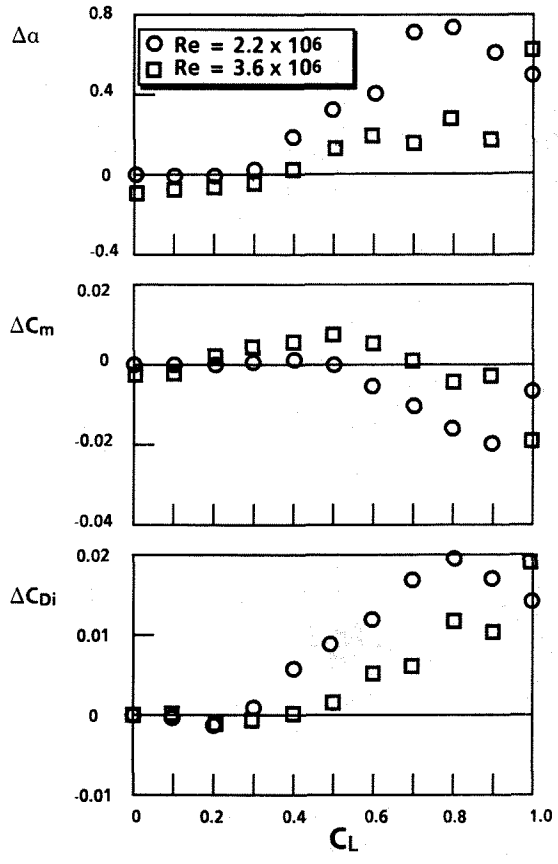

Figure 5. Reynolds Number Effect on Wall Interference for the A-10 Aircraft at M = 0.75.

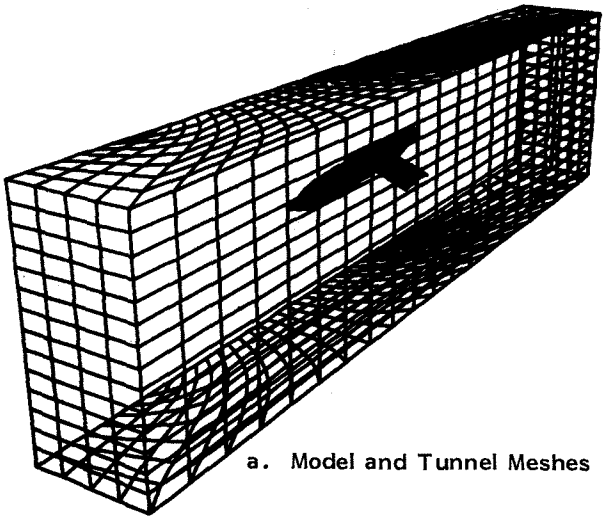

a. Model and Tunnel Meshes

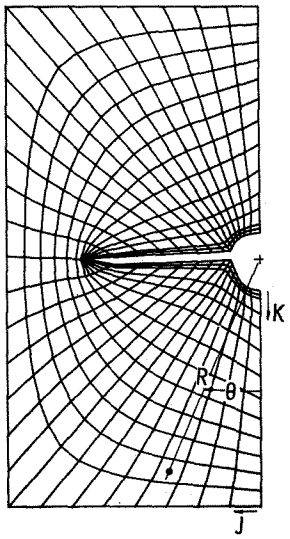

b. Cross Section of Computational Mesh

Figure 6. Typical Mesh for the Wall Interference Prediction Program.

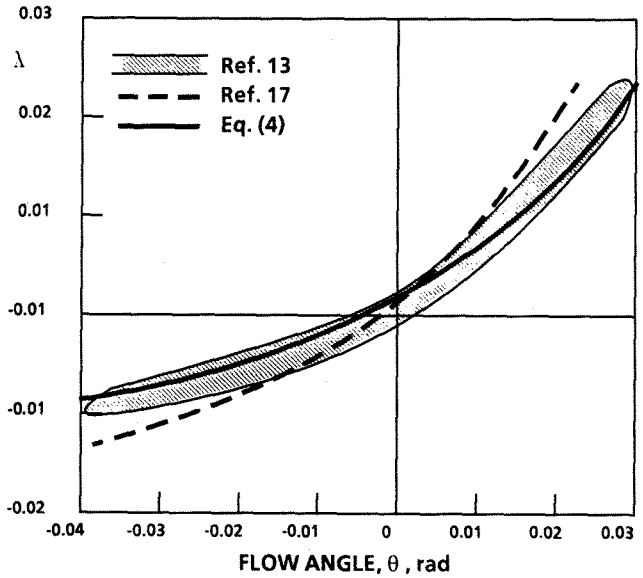

Figure 7. Relationship Between Flow Angle and Perforated Wall Mass Flux.

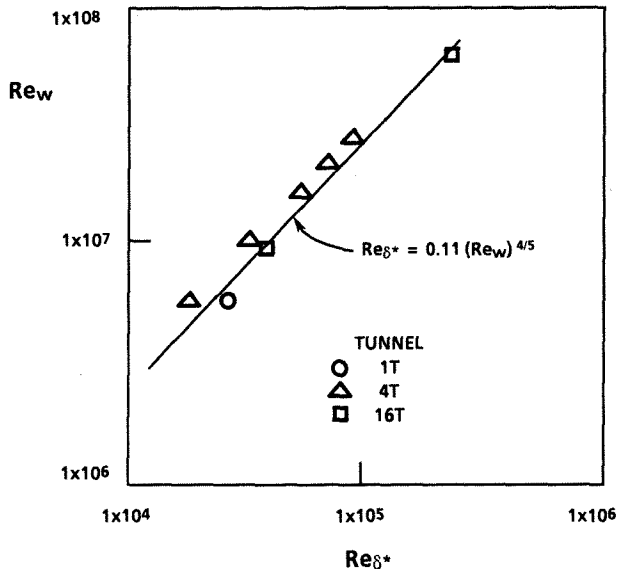

Figure 8. Test Section Entrance Displacement Thickness Correlation.

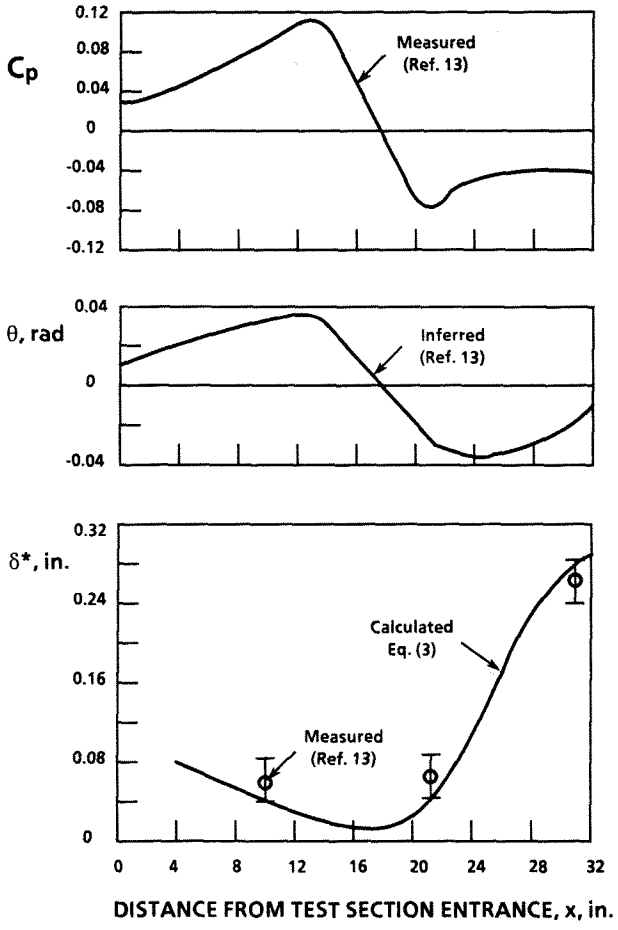

Figure 9. Validation of Boundary Layer Calculation Technique.

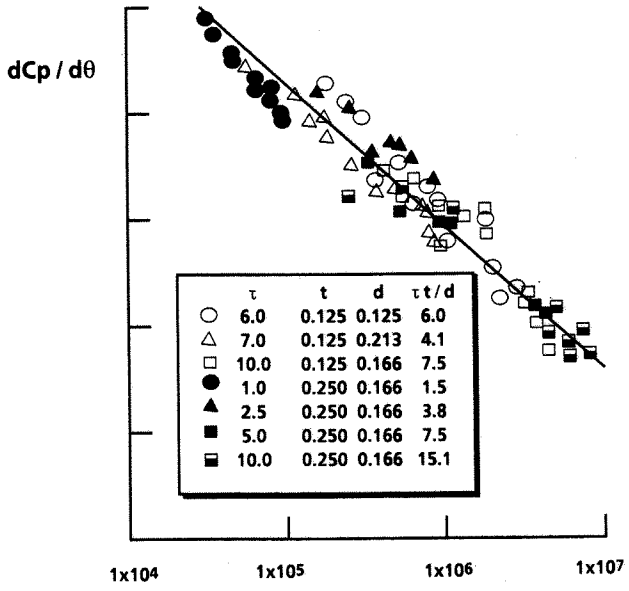

Figure 10. Perforated Wall Characteristic Data Correlation.

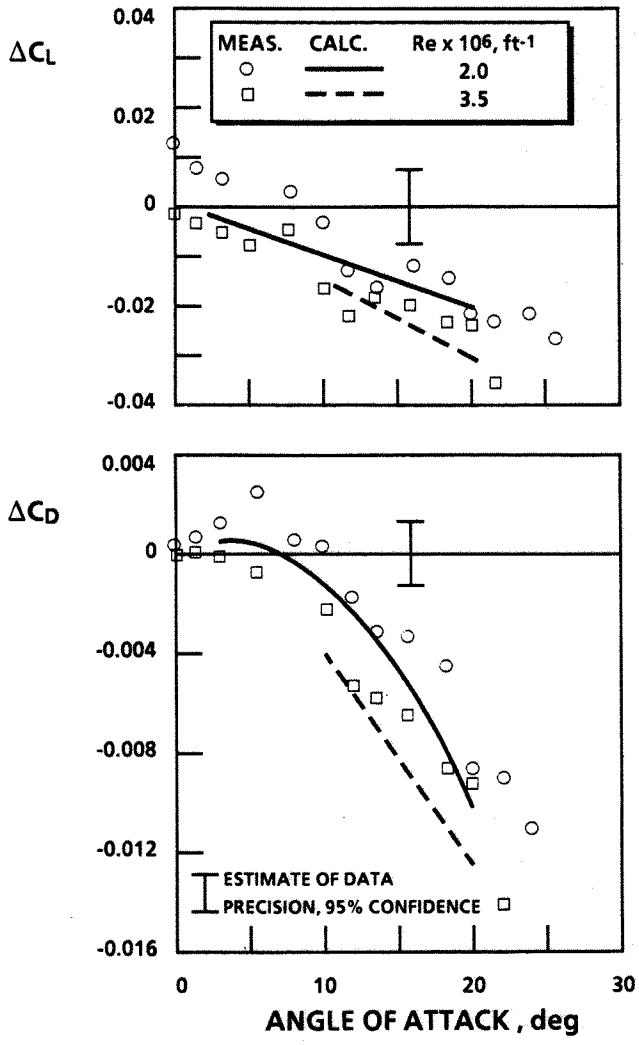

Figure 11. Wall Interference Prediction on a Typical Fighter Aircraft at M = 0.60.

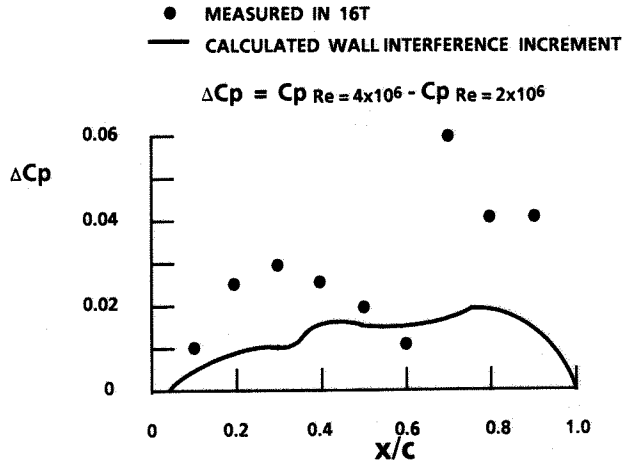

Figure 12. Prediction of Reynolds Number Effect on Wall Interference.

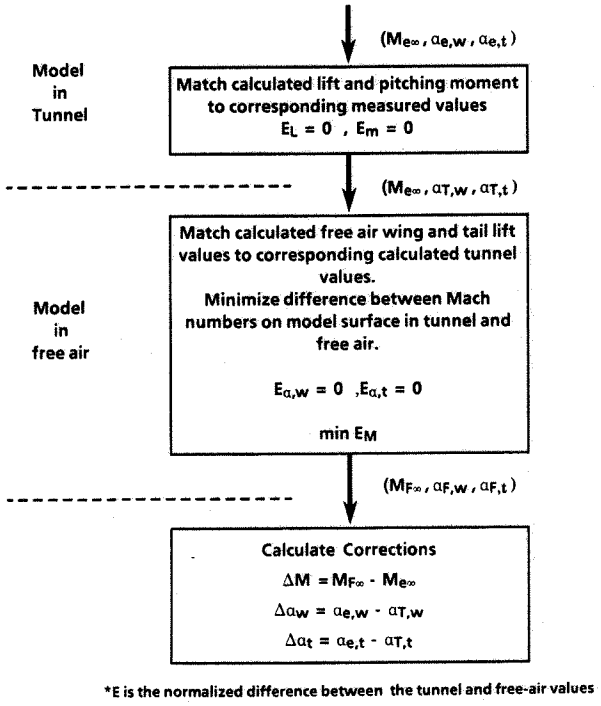

Figure 13. TUNCOR Code Correction Procedure.

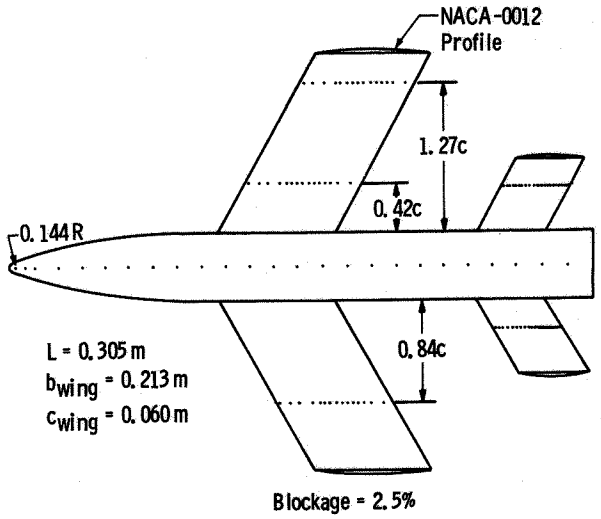

Figure 14. Generic Wall Interference Model.

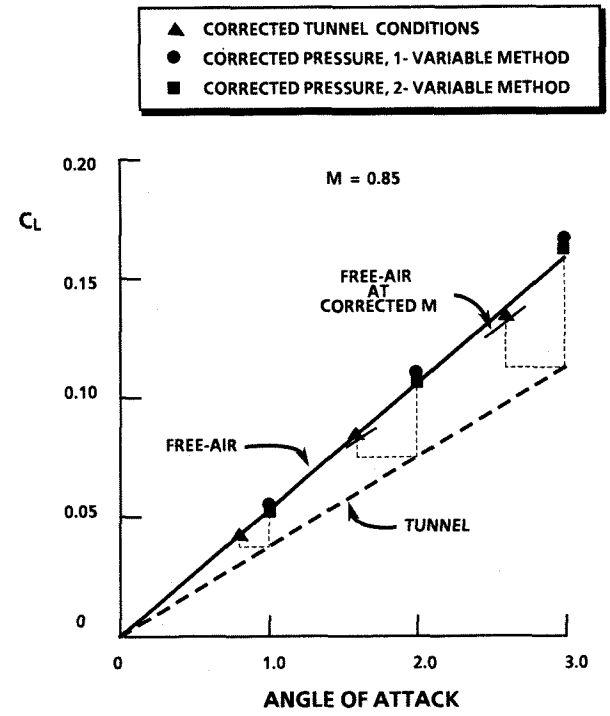

a. Lift Coefficient Correction

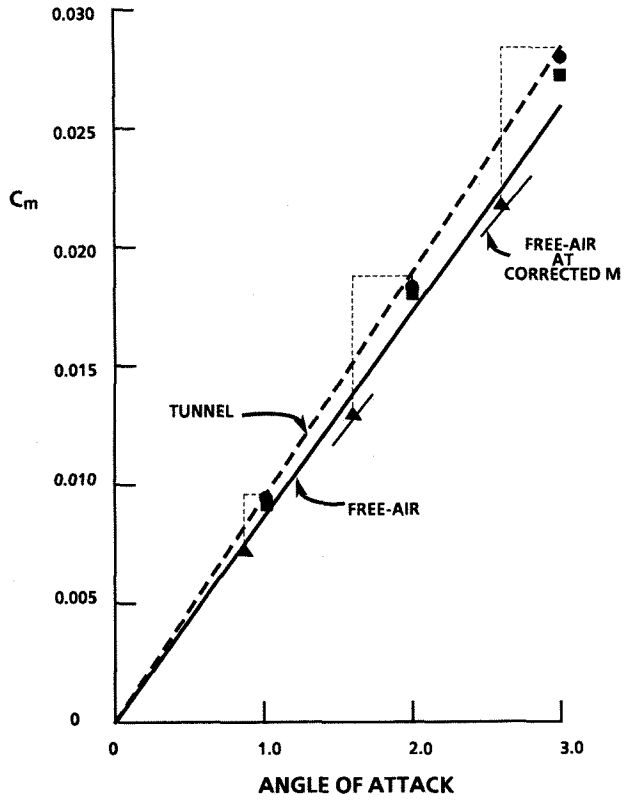

b. Pitching Moment Correction

Figure 15. Comparison of WIAC Techniques for the Wall Interference Model at M = 0.85.

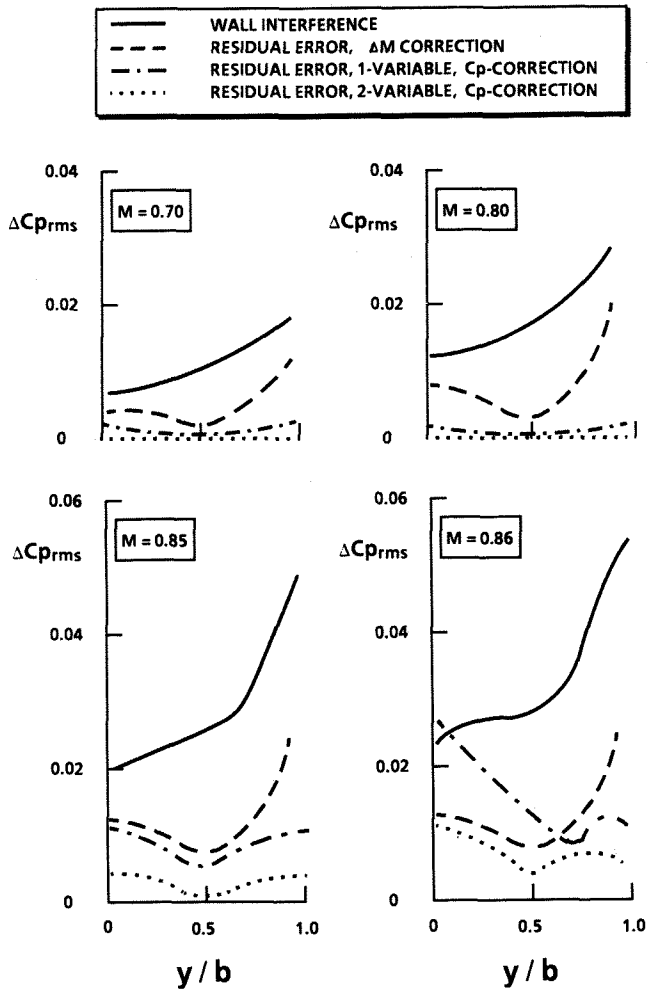

Figure 16. Evaluation of WIAC Techniques for Wing Alone at α = 0 deg.

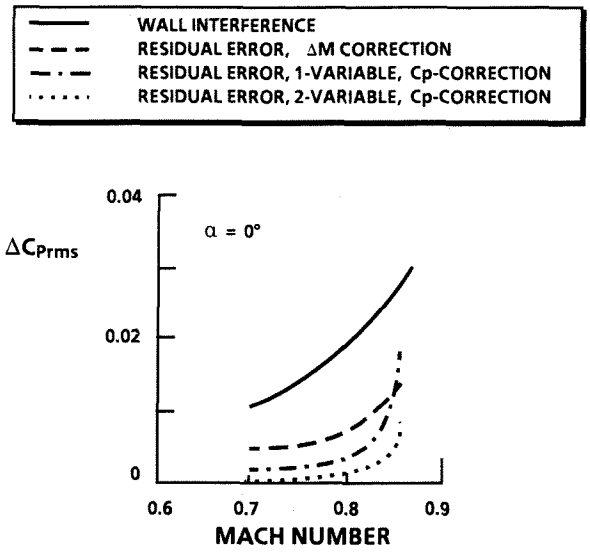

Figure 17. Variation of the Residual Error for Various WIAC Techniques for Wing Alone Model at α = 0 deg.

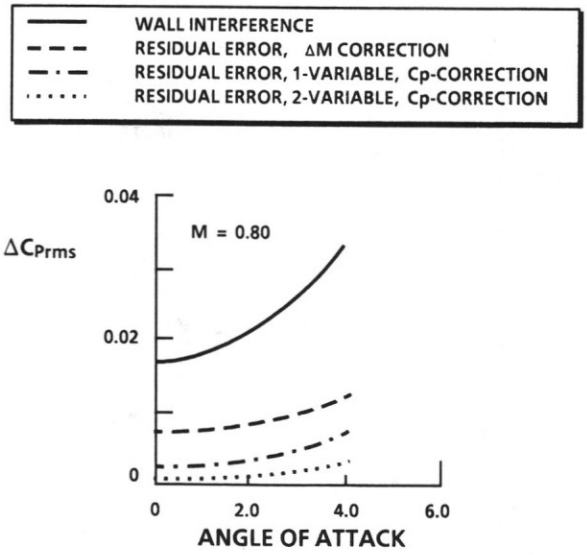

Figure 18. Variation with Angle of Attack of the Residual Error for Various WIAC Techniques.

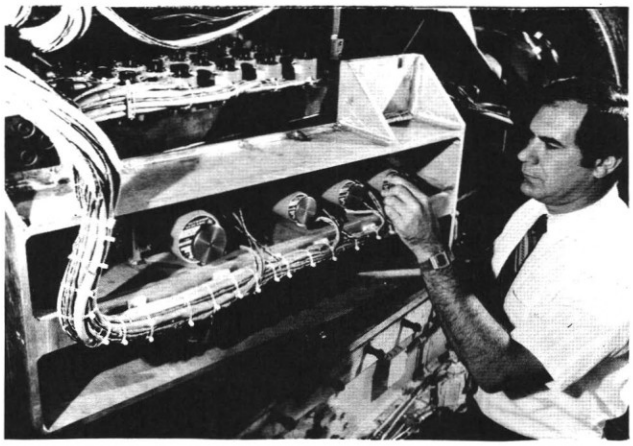

Figure 19. 1T Adaptive Walls.

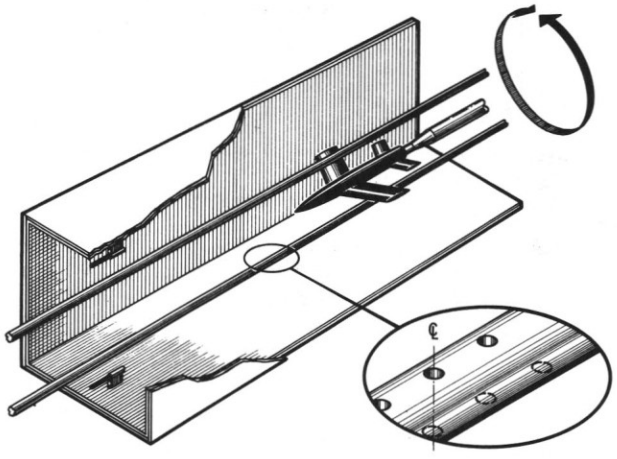

Figure 20. Interface Measurement System.

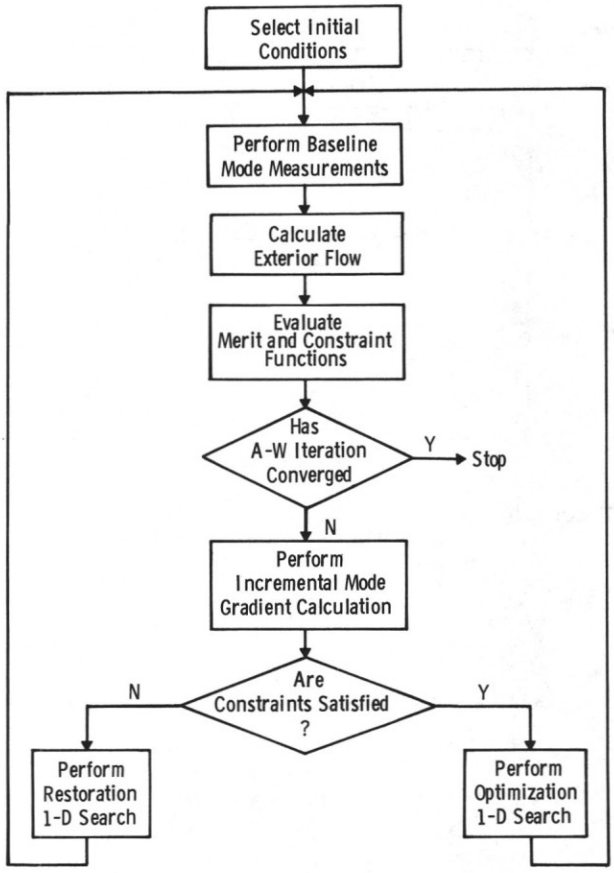

Figure 21. Automated Adaptive-Wall Iterative Procedure.

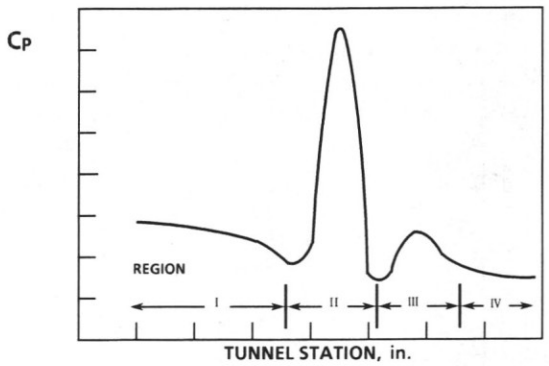

Figure 22. Typical Interface Pressure Distribution and the Critical Regions.

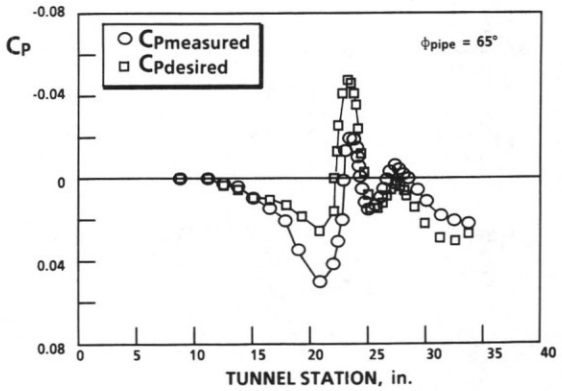

Figure 23. Interface Pressure Distribution for Baseline, M = 0.90 and α = 4 deg.

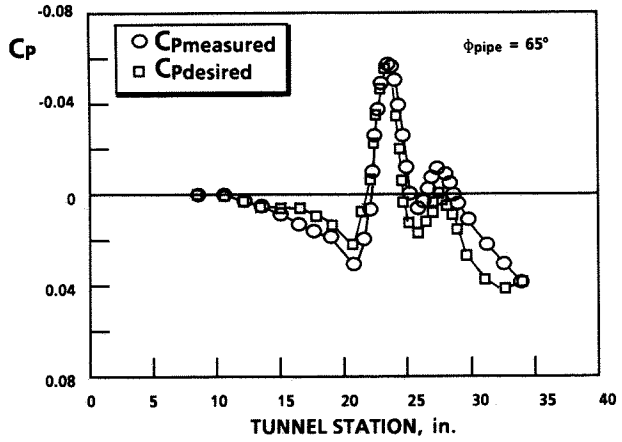

Figure 24. Interface Pressure Distribution for Wing Region Optimization, M = 0.90 and α = 4 deg.

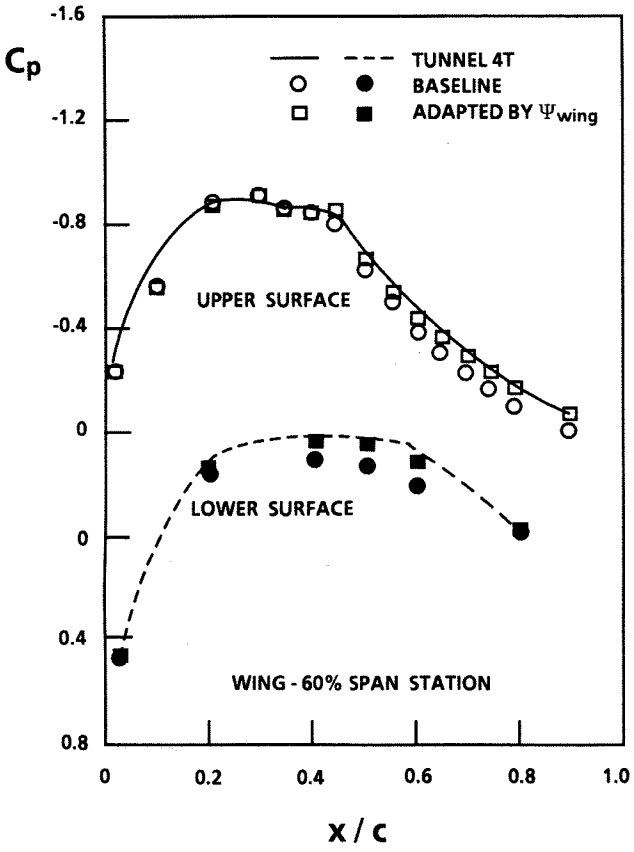

a. Wing

Figure 25. Model Pressure Distribution for Wing Region Optimization, M = 0.90 and α = 4 deg.

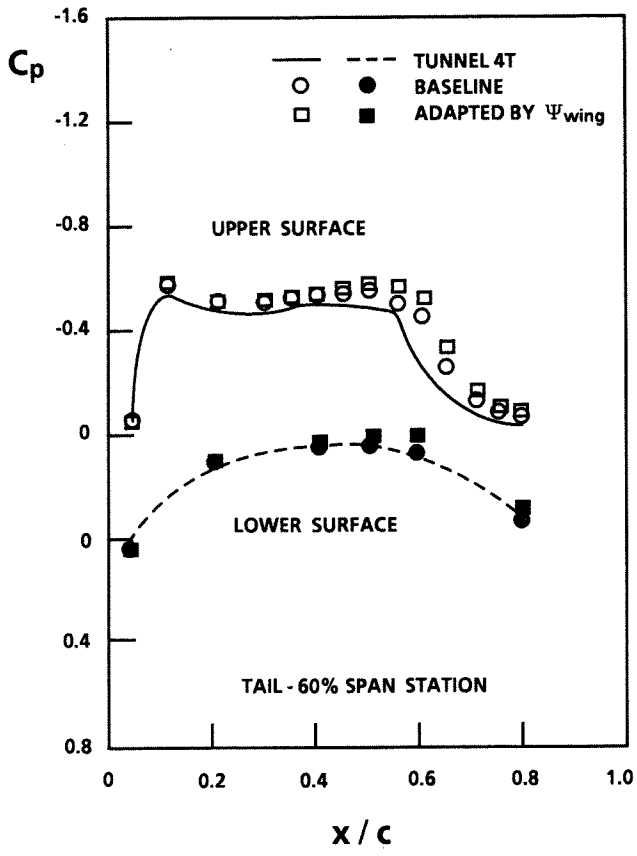

b. Tail

Figure 25. Concluded.

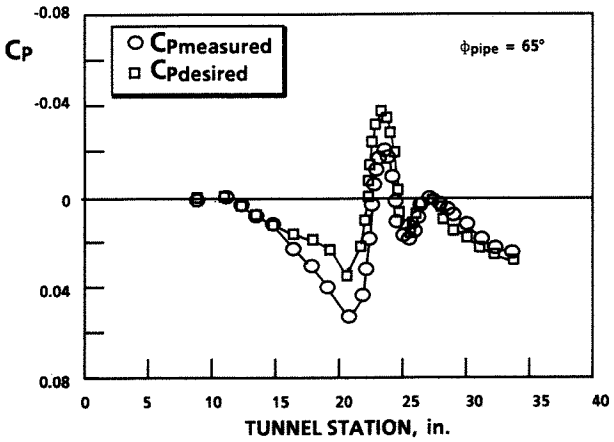

Figure 26. Interface Pressure Distribution for Tail Region Optimization, M = 0.90 and α = 4 deg.

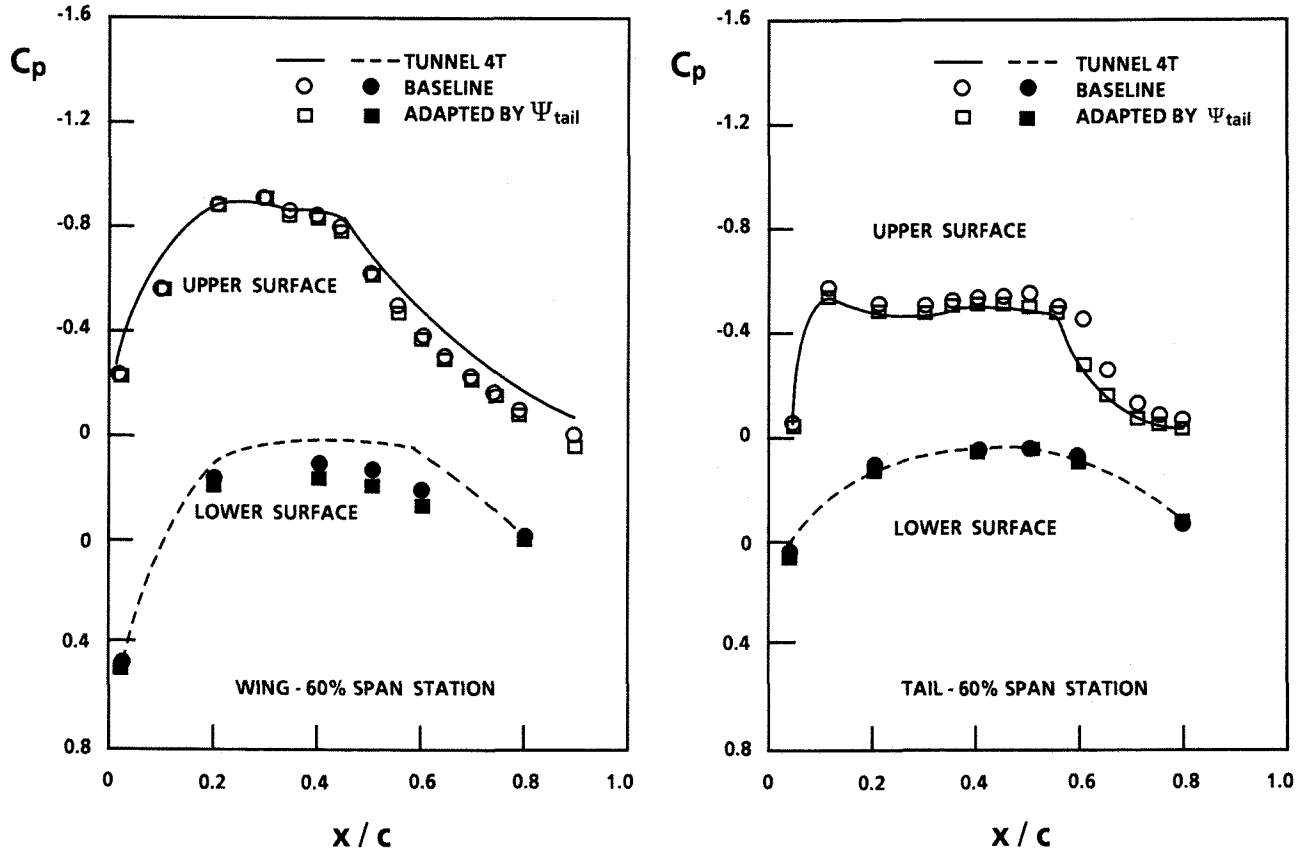

a. Wing

b. Tail

Figure 27. Model Pressure Distribution for Tail Region Optimization, M = 0.90 and α = 4 deg.

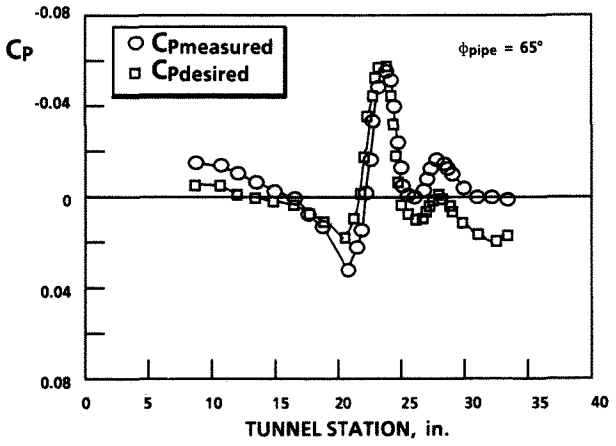

Figure 28. Interface Pressure Distribution for Tail-Then-Wing Region Optimization, M = 0.90 and α = 4 deg.

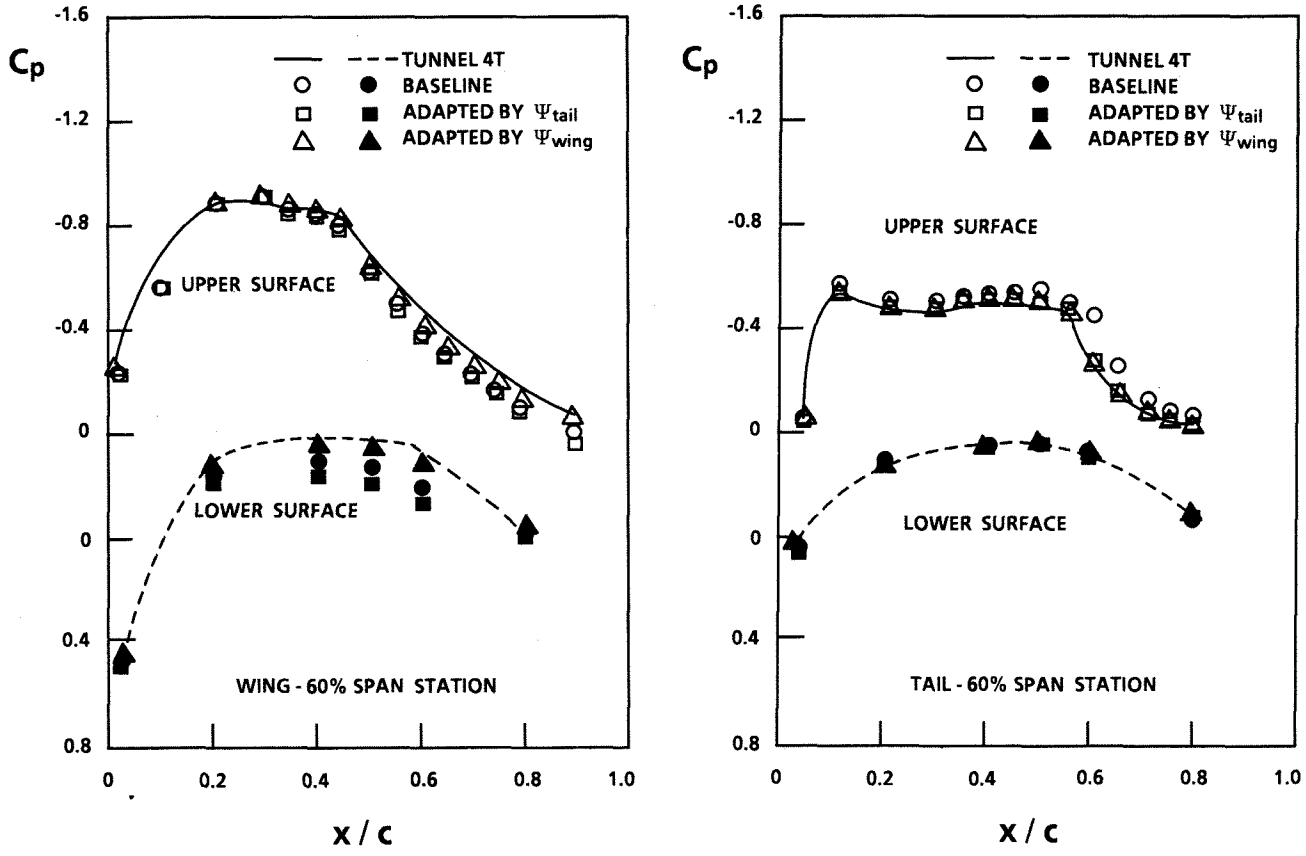

a. Wing

b. Tail

Figure 29. Model Pressure Distribution for Tail-Then-Wing Region Optimization, M = 0.90 and α = 4 deg.